Electronic Supplementary Material (ESI) for RSC Advances

"Click" chemistry toward *bis*(DOTA-derived) heterometallic complexes: potential bimodal MRI/PET(SPECT) molecular probes.

Mojmír Suchý,[a,b] Robert Bartha[b] and Robert H. E. Hudson[a]

[a]*Department of Chemistry, The University of Western Ontario, London, Ontario, Canada*
[b]*Robarts Research Institute, The University of Western Ontario, London, Ontario, Canada*

Contents:

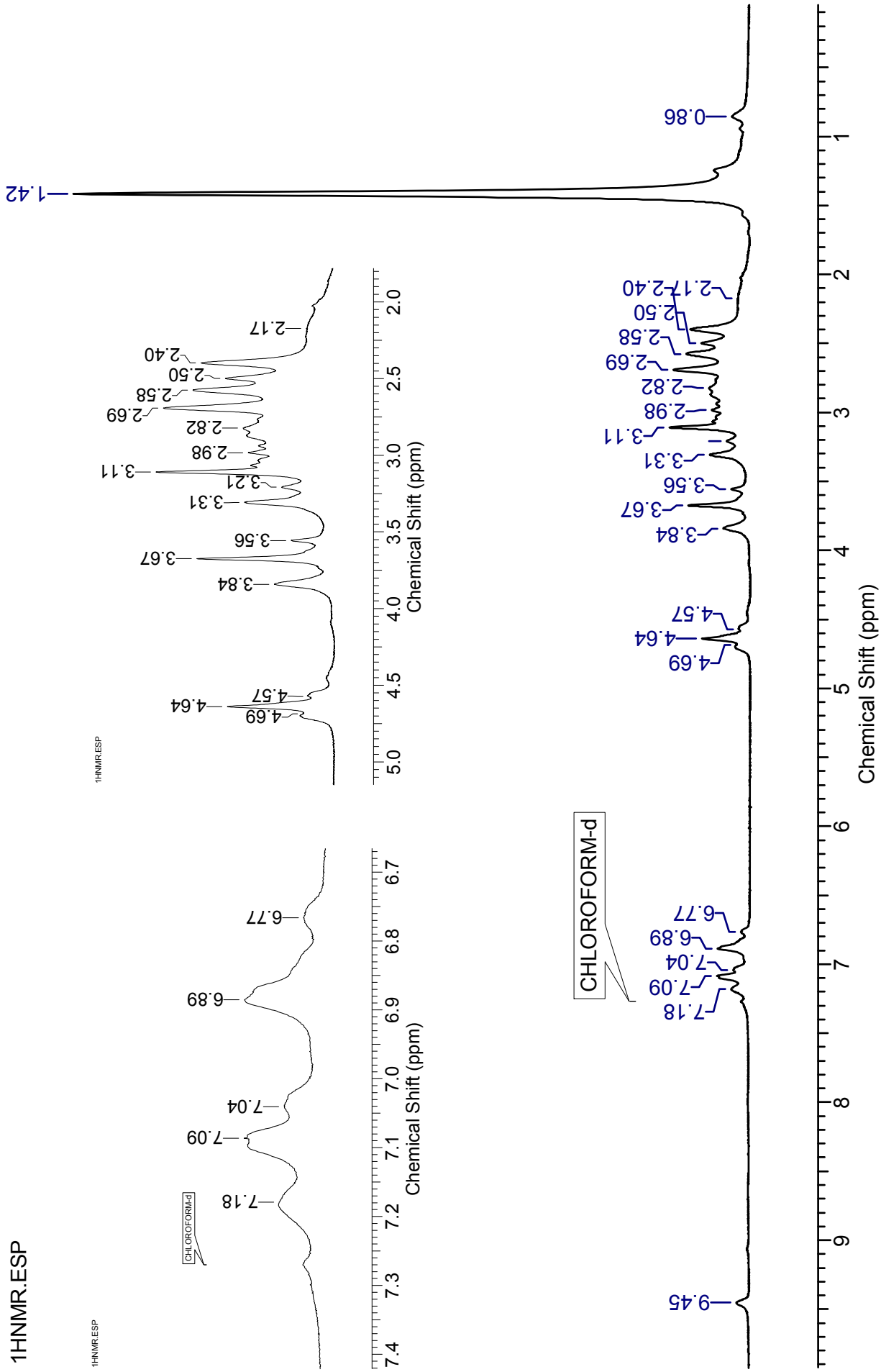

Figure S1: ^{1}H NMR spectrum ($CDCl_3$) of compound **6a**.

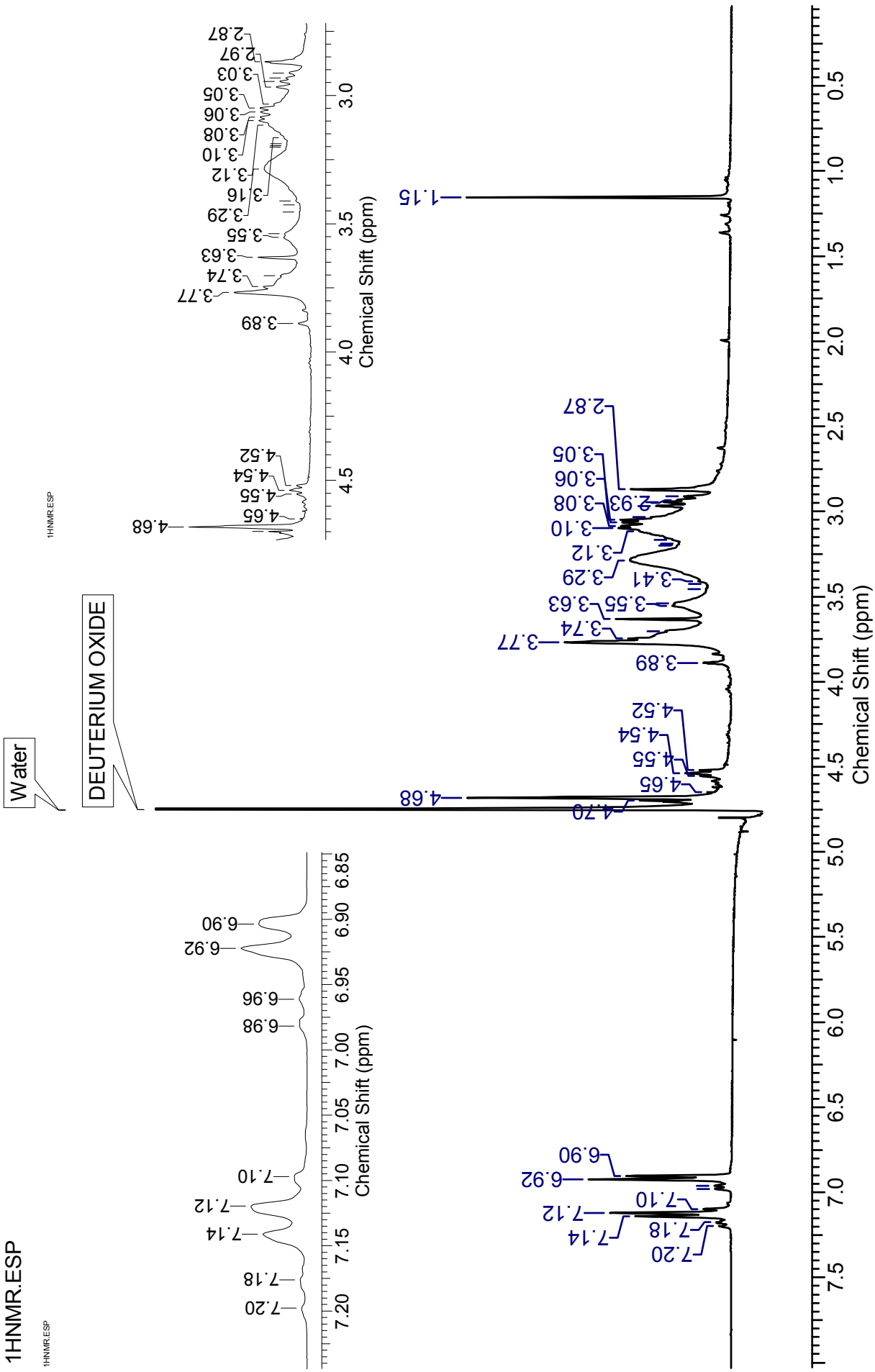

Figure S2: ^{1}H NMR spectrum ($CDCl_3$) of an unmetallated version of complex **6b**.

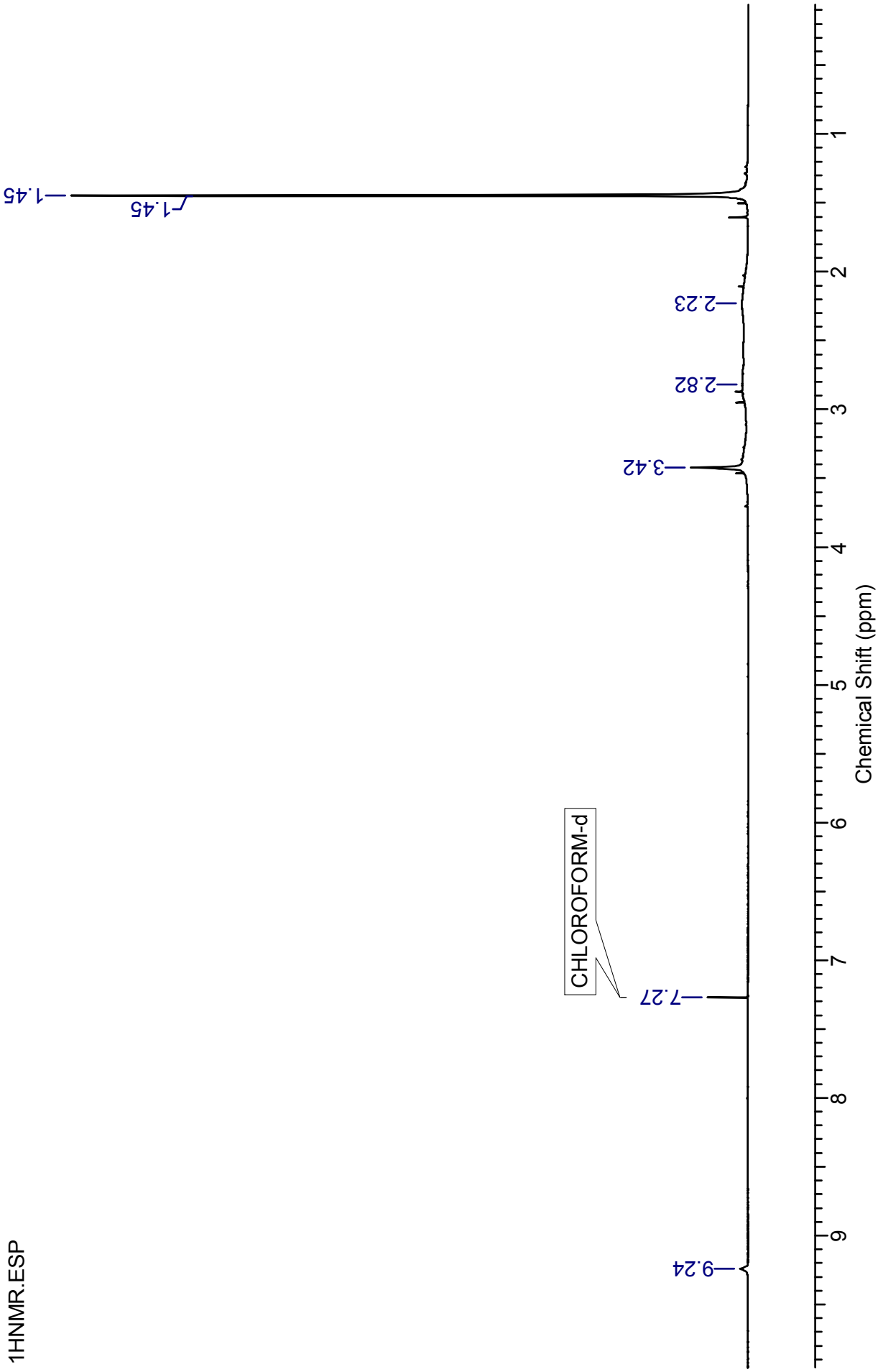

Figure S3: ^{1}H NMR spectrum ($CDCl_3$) of compound **7a**

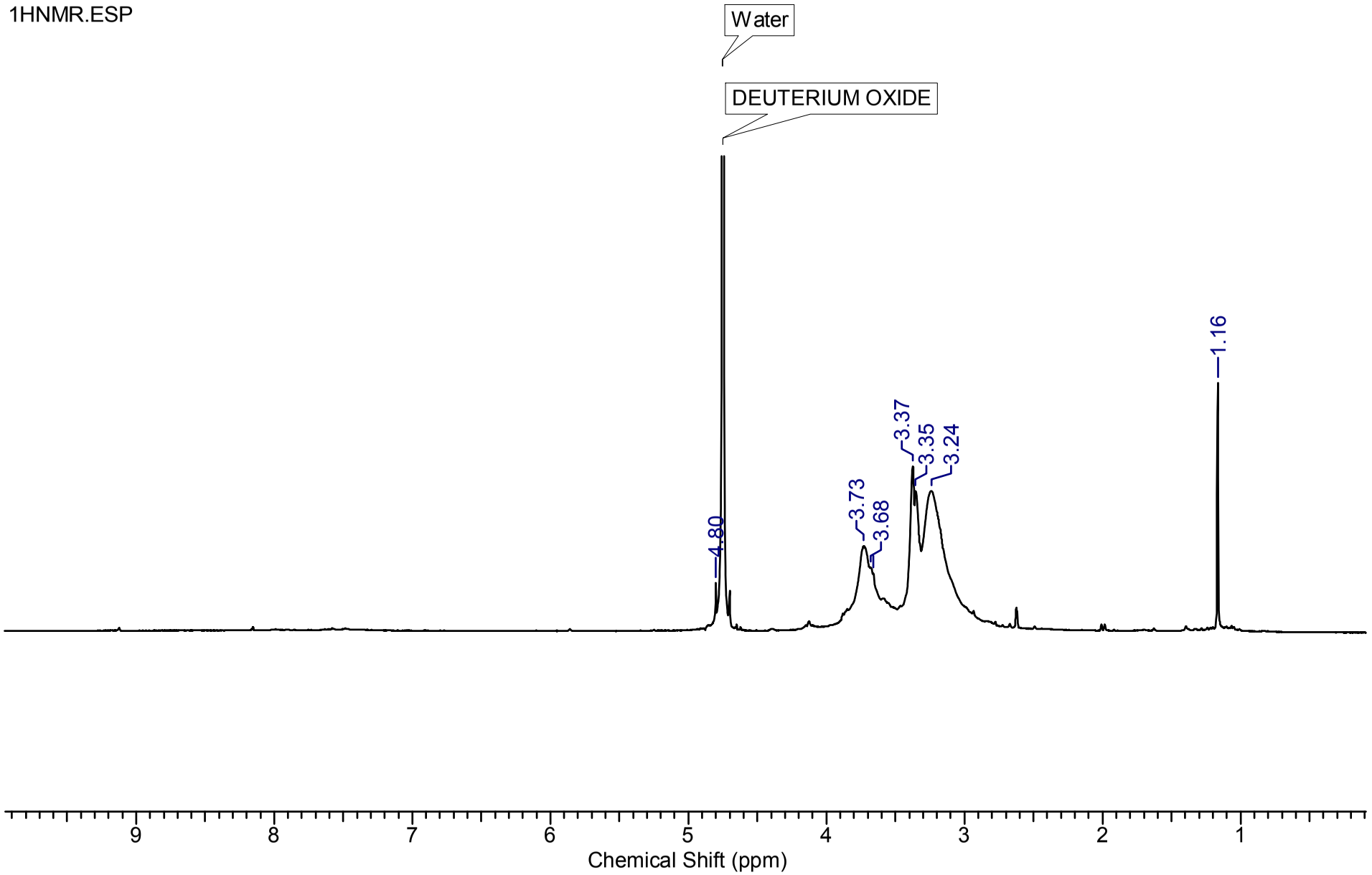

Figure S4: ^{1}H NMR spectrum (D_2O) of an ester deprotected version of ligand **7a**.

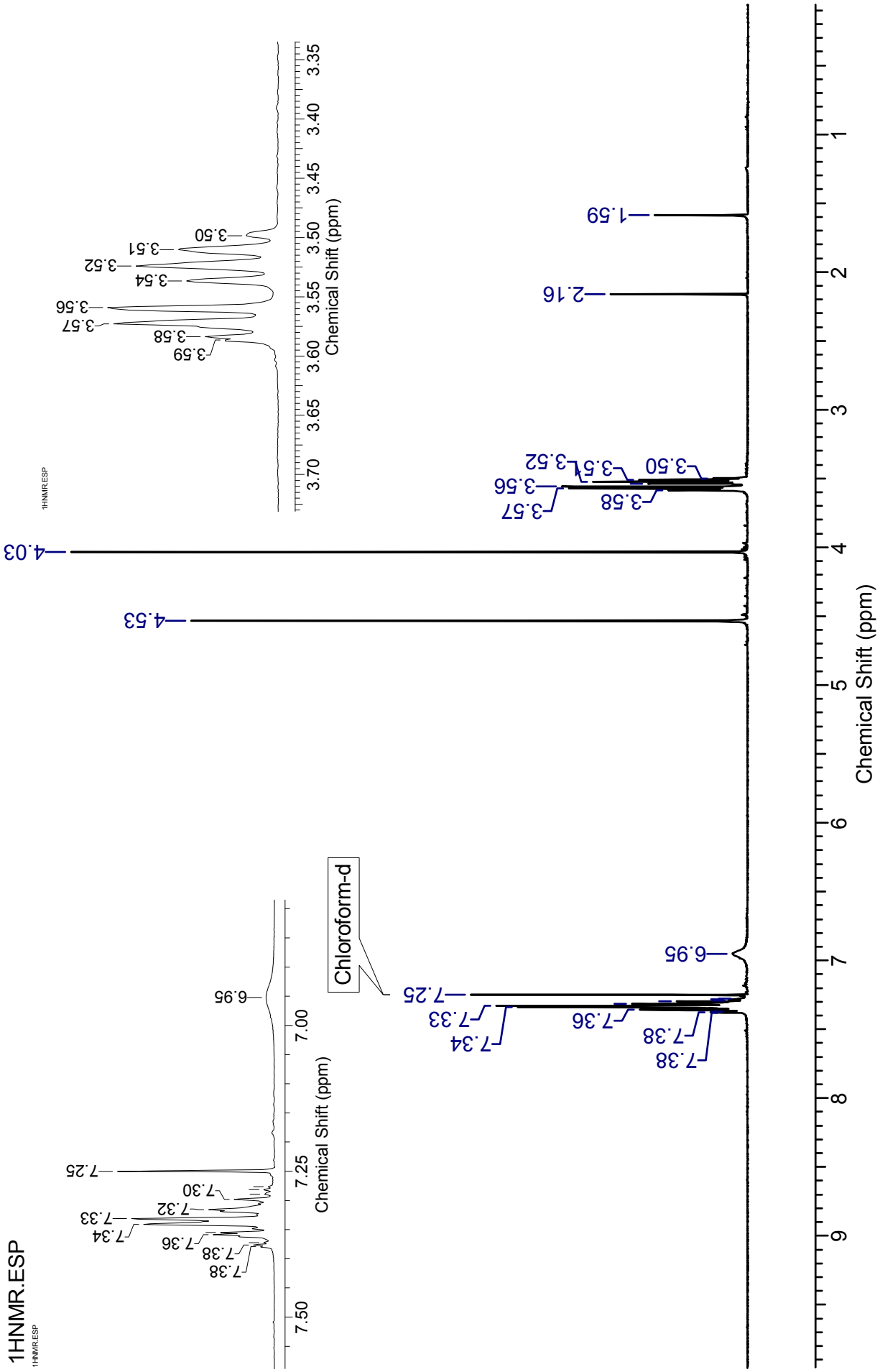

Figure S5: ^{1}H NMR spectrum ($CDCl_3$) of compound **12**.

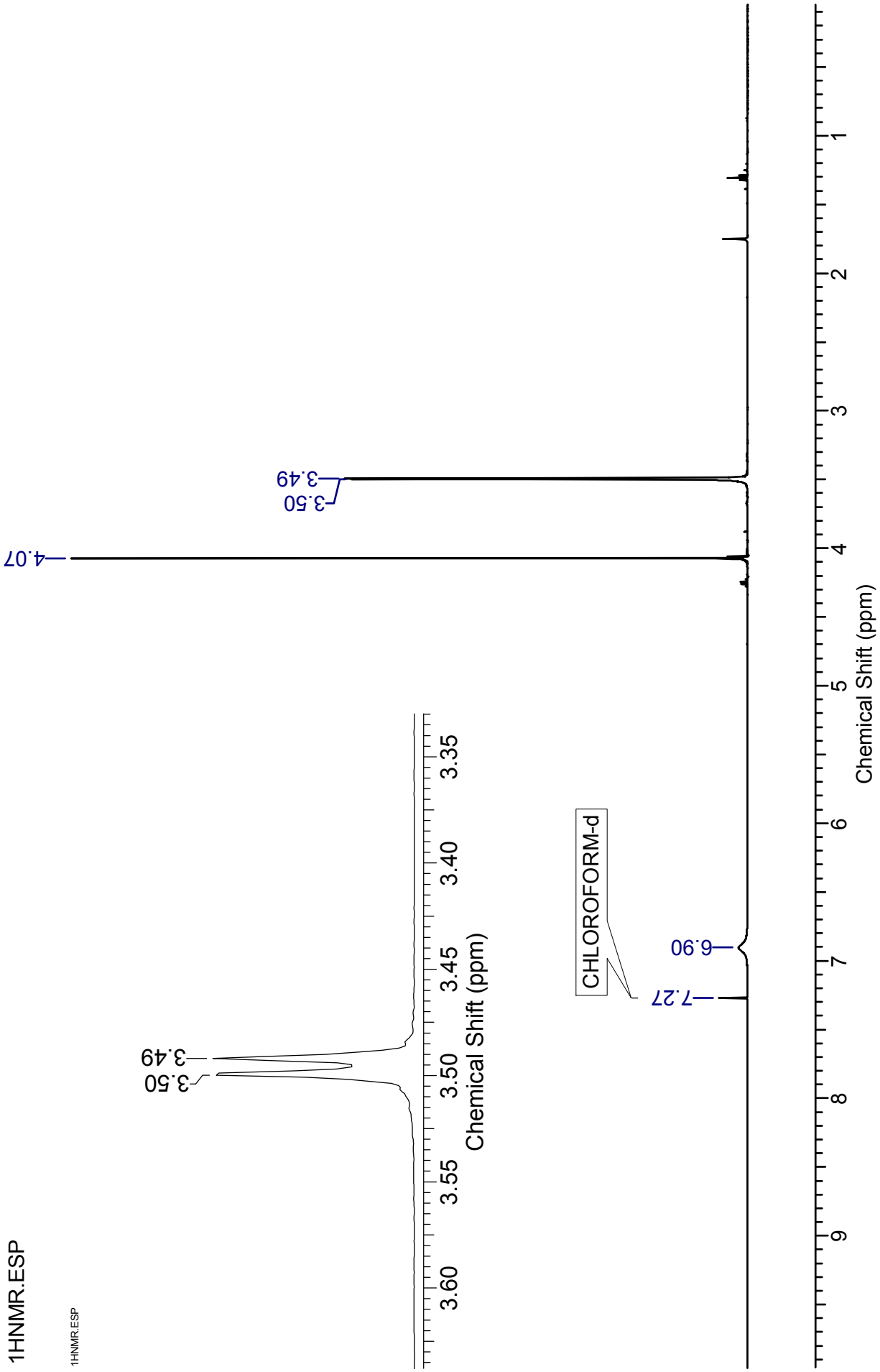

Figure S6: ^{1}H NMR spectrum ($CDCl_3$) of compound **15**.

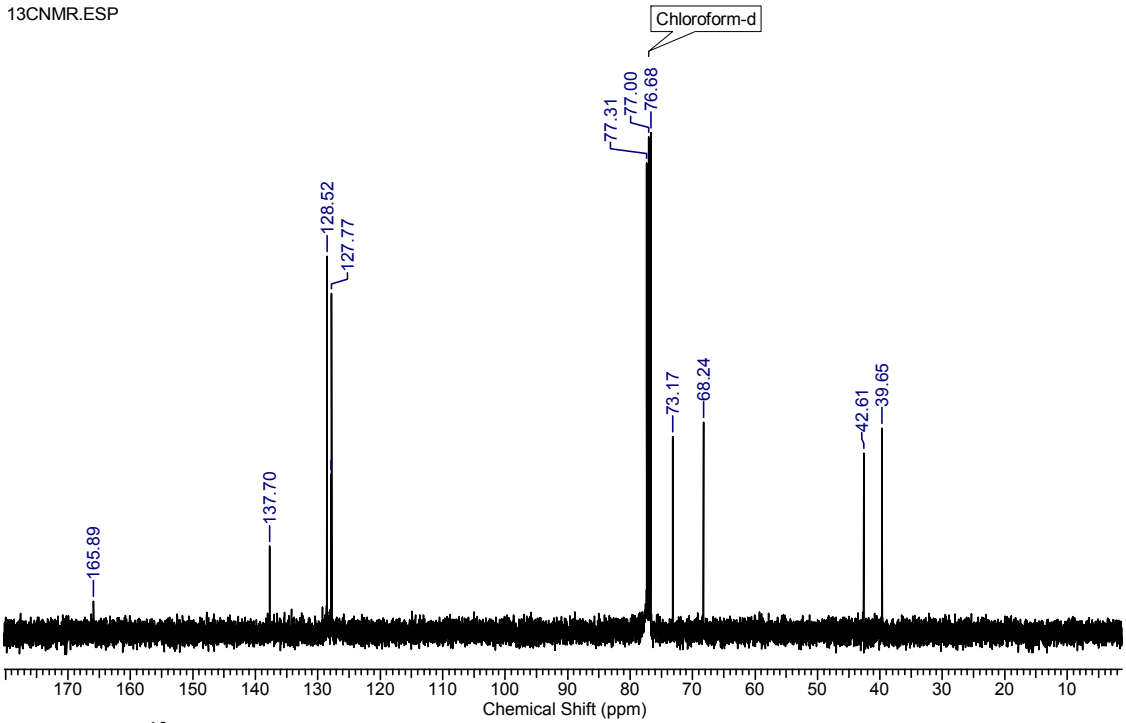

Figure S7: ^{13}C NMR spectrum ($CDCl_3$) of compound **12**.

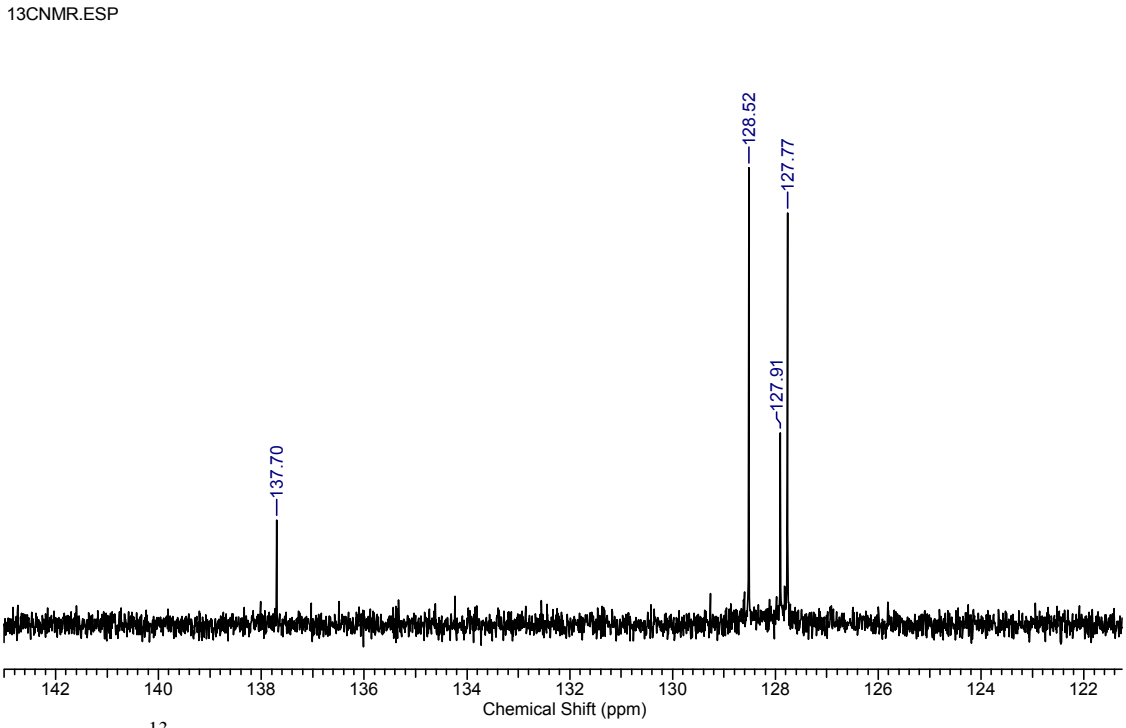

Figure S8: ^{13}C NMR spectrum ($CDCl_3$) of compound **12**, an expansion of the aromatic carbon region.

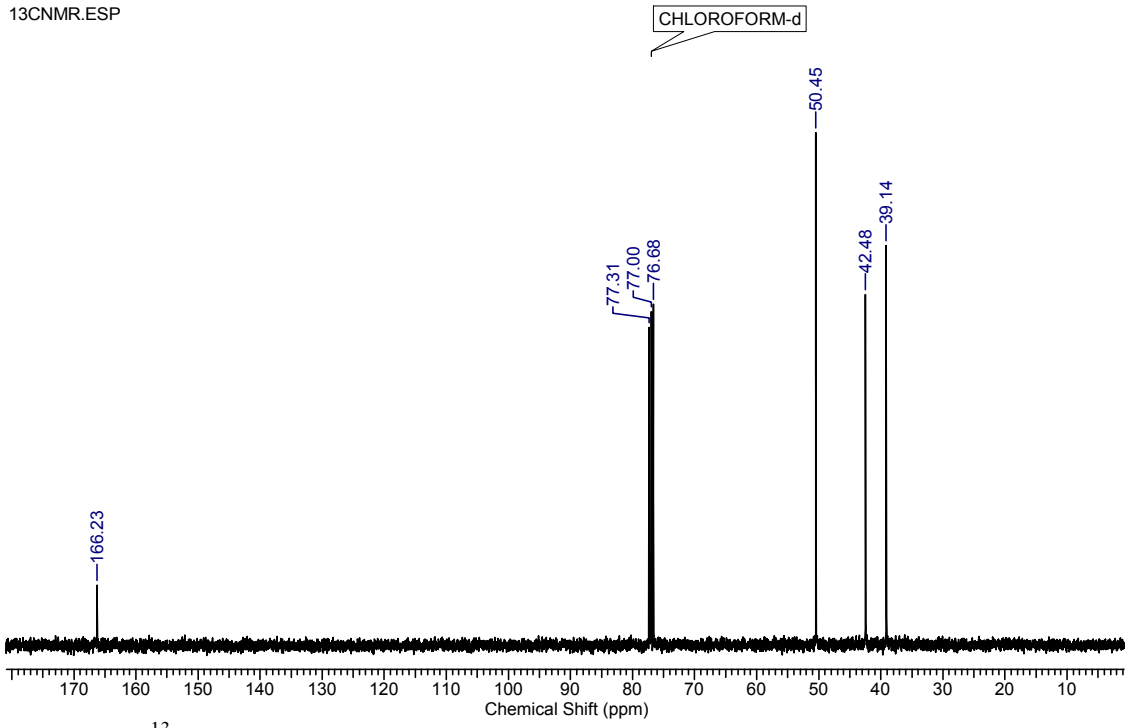

Figure S9: ^{13}C NMR spectrum ($CDCl_3$) of compound **15**.

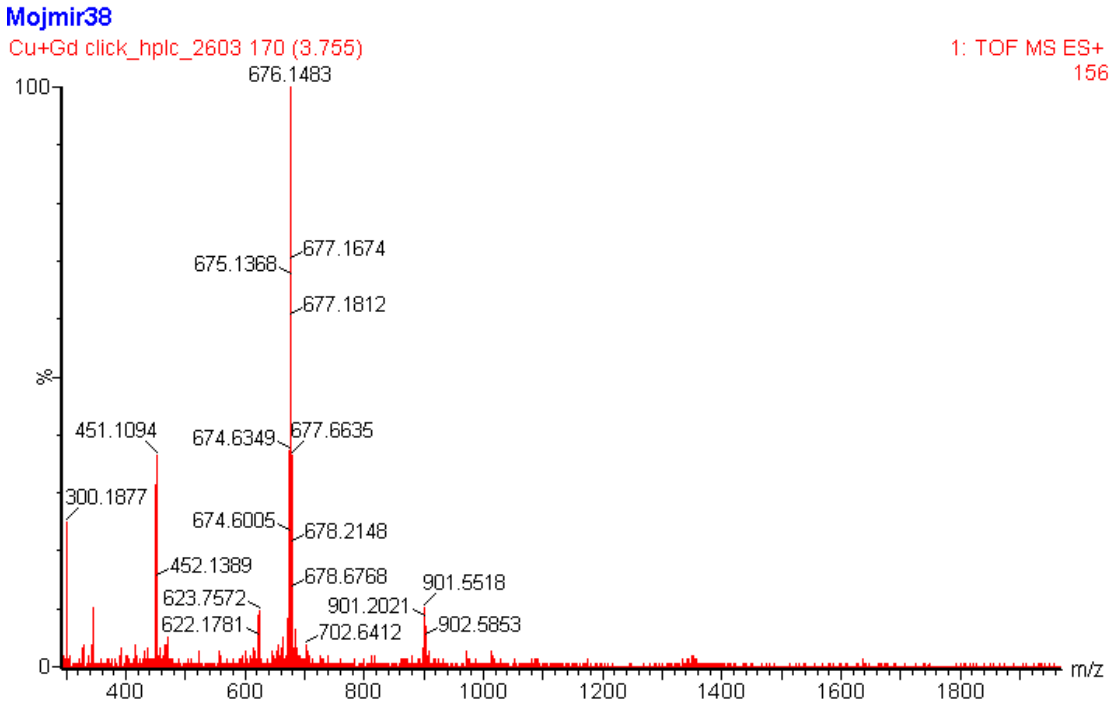

Figure S10: HR-ESI-MS spectrum of compound **5a** showing a proper charge state envelope.

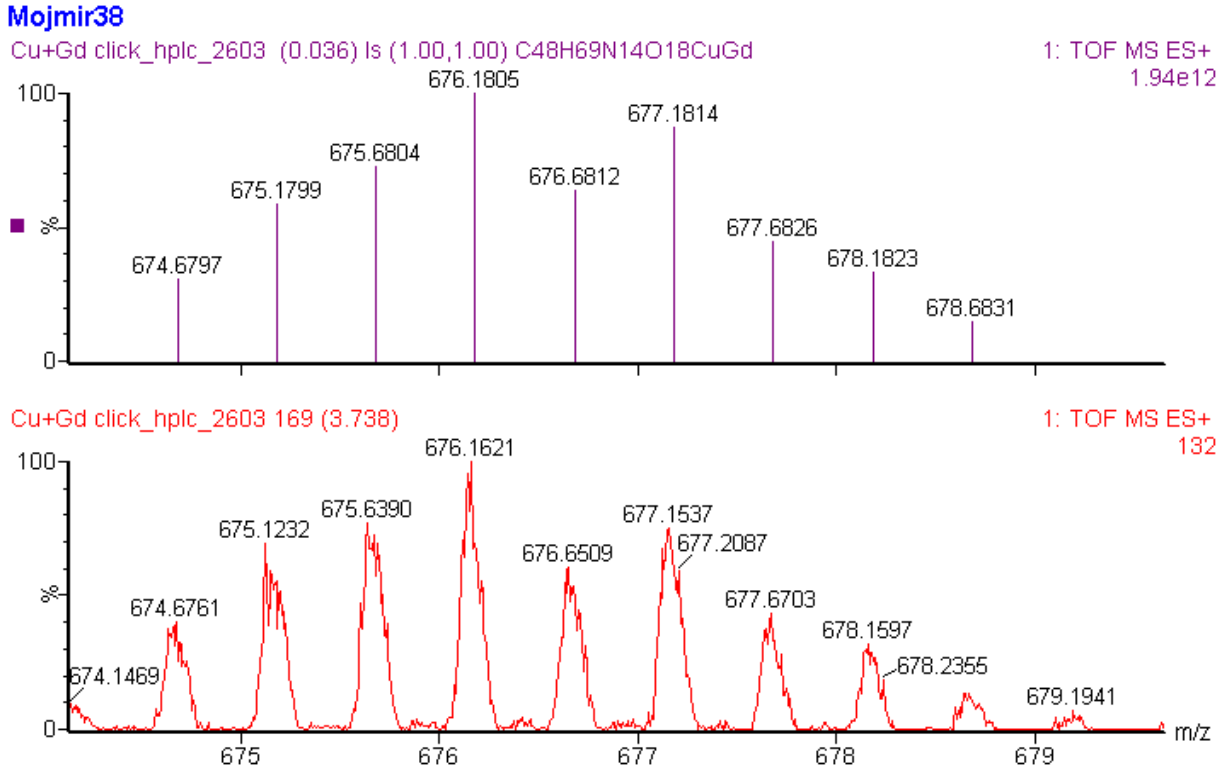

Figure S11: HR-ESI-MS spectrum of compound **5a**, M^{2+} charge state observed (bottom) spectrum and calculated (top) spectrum, note the isotope pattern due to the presence of heavy metals.

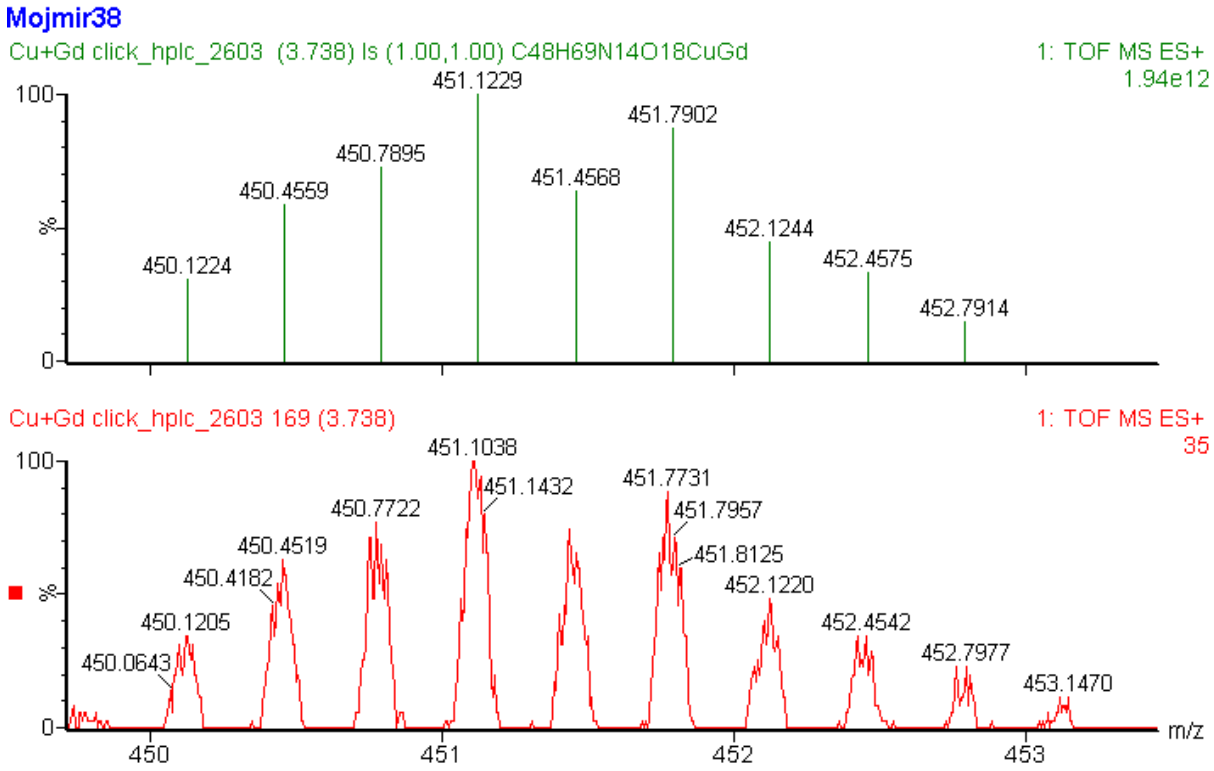

Figure S12: HR-ESI-MS spectrum of compound **5a**, M^{3+} charge state observed (bottom) spectrum and calculated (top) spectrum, note the isotope pattern due to the presence of heavy metals.

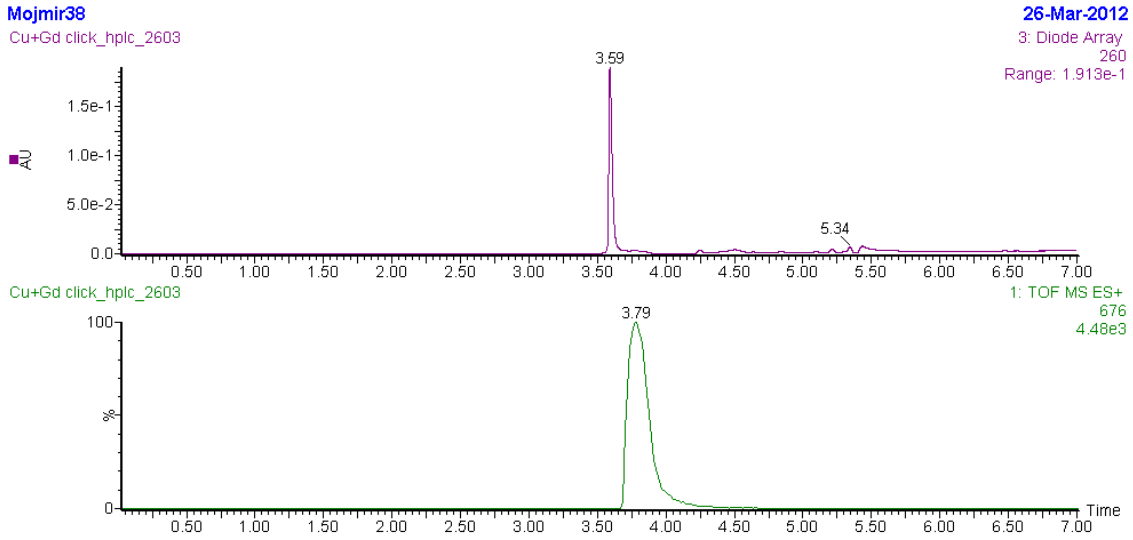

Figure S13: UPLC chromatograms (Method B) of compound **5a**, MS detector (bottom), UV detector (top).

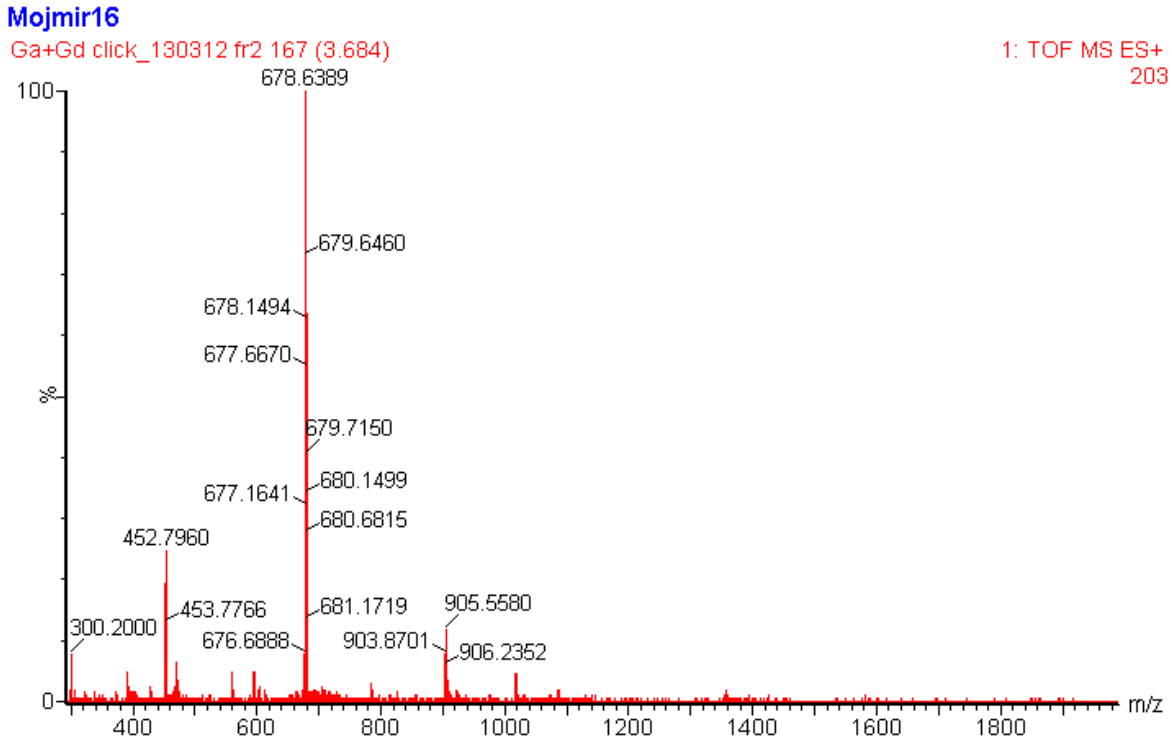

Figure S14: HR-ESI-MS spectrum of compound **5b** showing a proper charge state envelope.

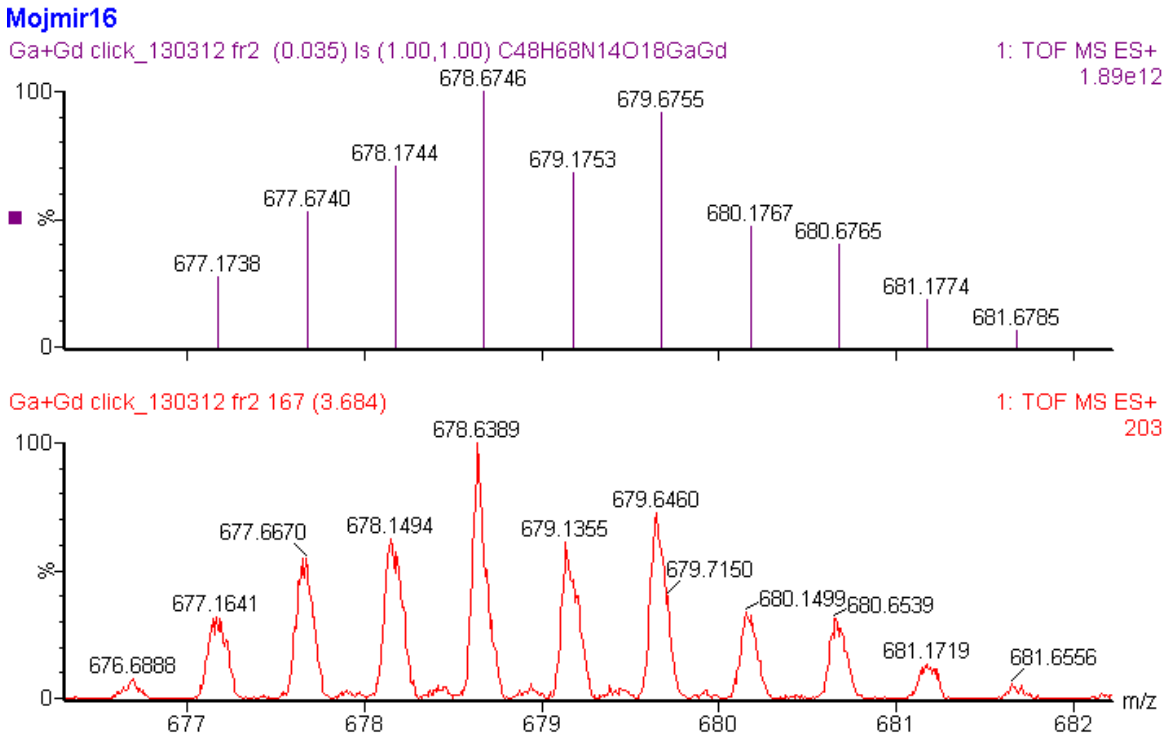

Figure S15: HR-ESI-MS spectrum of compound **5b**, M^{2+} charge state observed (bottom) spectrum and calculated (top) spectrum, note the isotope pattern due to the presence of heavy metals.

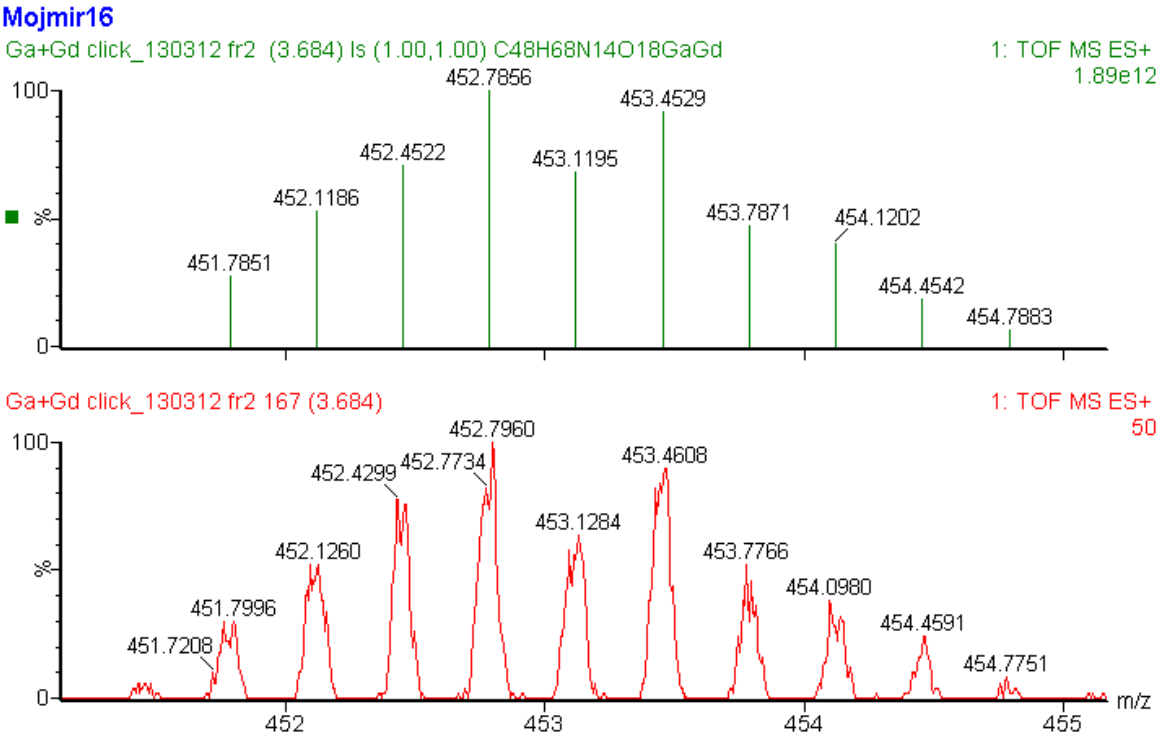

Figure S16: HR-ESI-MS spectrum of compound **5b**, M^{3+} charge state observed (bottom) spectrum and calculated (top) spectrum, note the isotope pattern due to the presence of heavy metals.

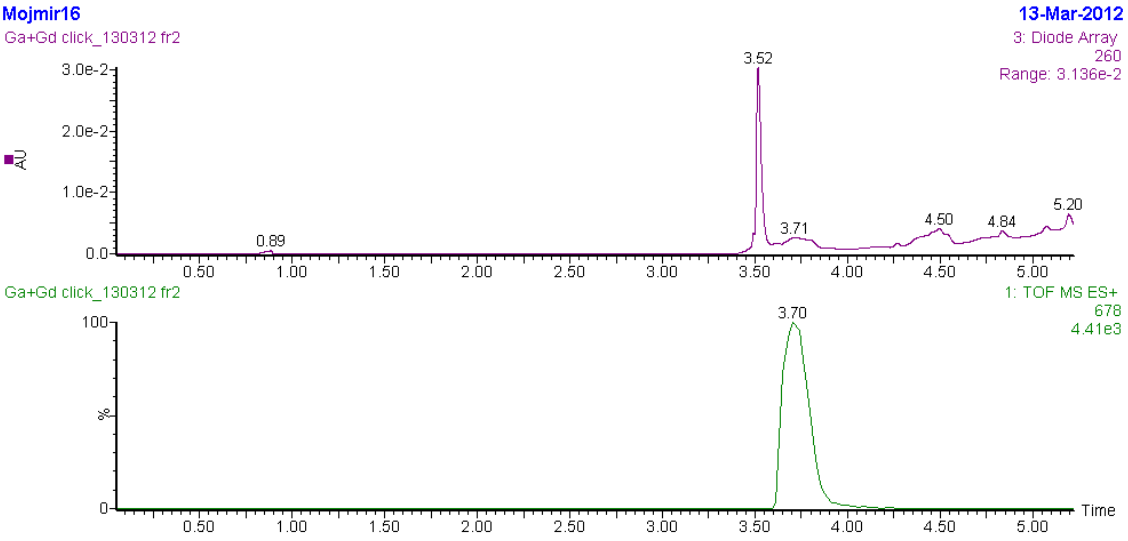

Figure S17: UPLC chromatograms (Method B) of compound **5b**, MS detector (bottom), UV detector (top).

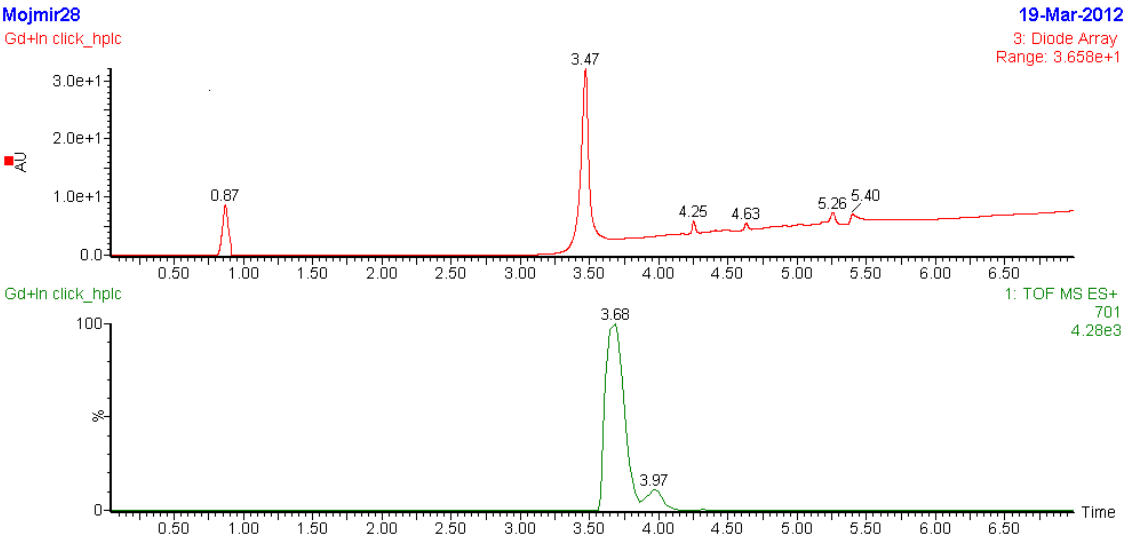

Figure S18: UPLC chromatograms (Method B) of compound **5d**, MS detector (bottom), UV detector (top). The remaining MS data for compound **5d** are shown in the body of the paper (Figure 2).

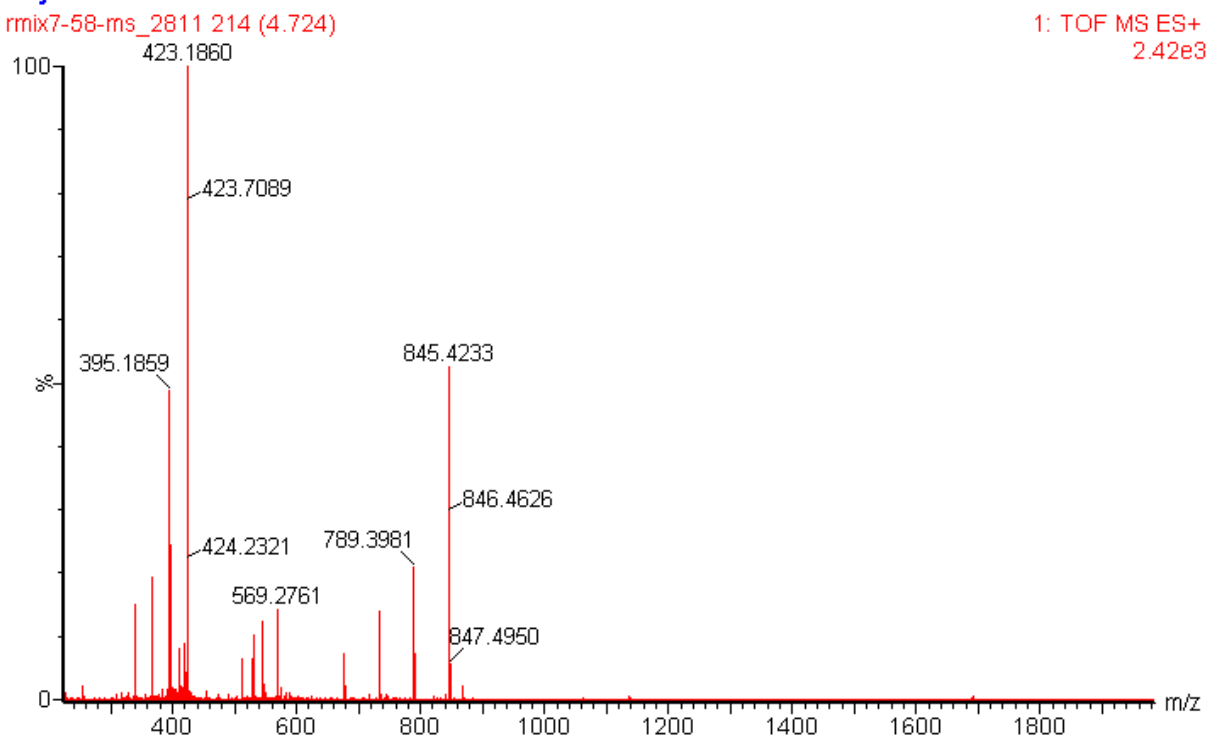

Figure S19: HR-ESI-MS spectrum of compound **6a** showing a proper charge state envelope. The *t*-Bu ester functionalities present in **6a** are not stable under the conditions of the analysis therefore M^+-56, M^+-112 and M^+-168 ions are observed for the singly charged species and M^+-28, M^+-56 and M^+-84 ions are observed for the doubly charged species.

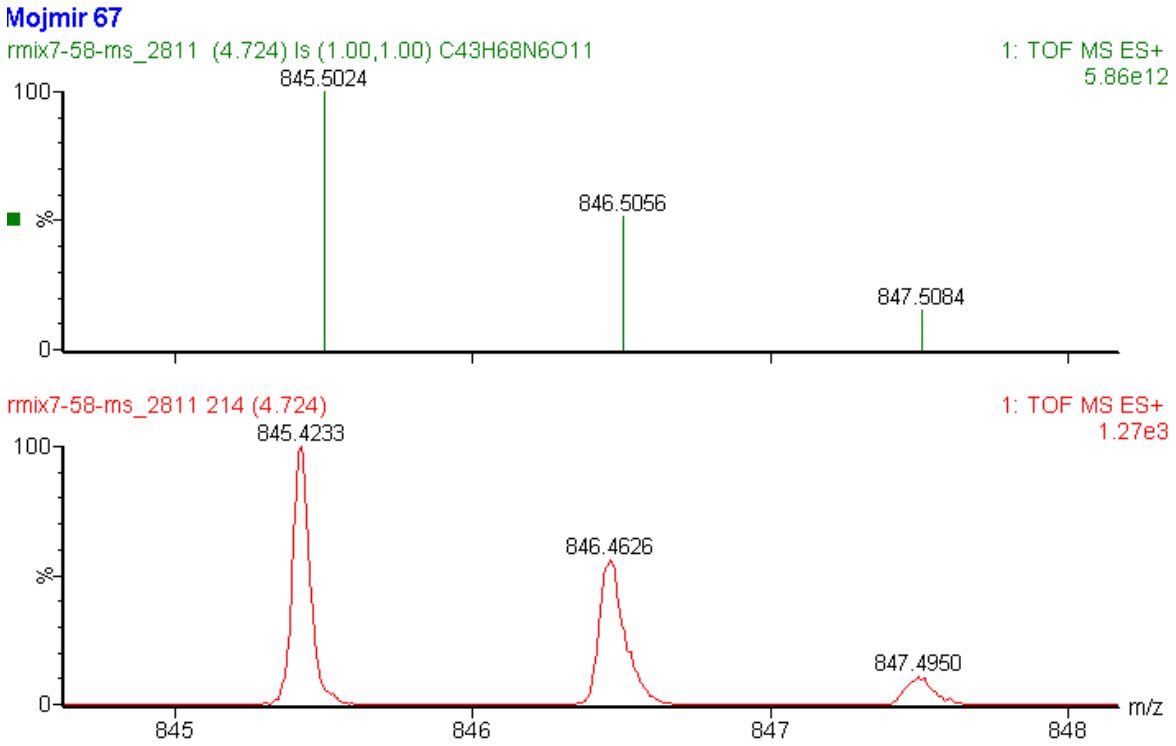

Figure S20: HR-ESI-MS spectrum of compound **6a**, M^{+} charge state observed (bottom) spectrum and calculated (top) spectrum.

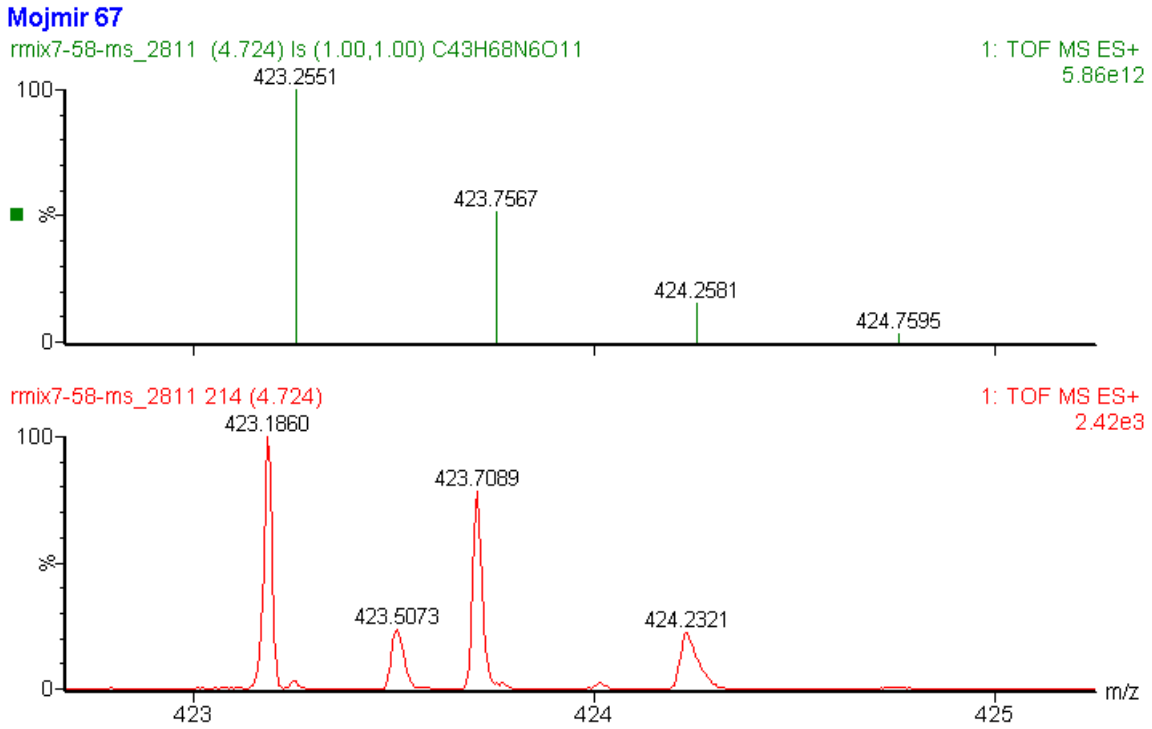

Figure S21: HR-ESI-MS spectrum of compound **6a**, M^{2+} charge state observed (bottom) spectrum and calculated (top) spectrum.

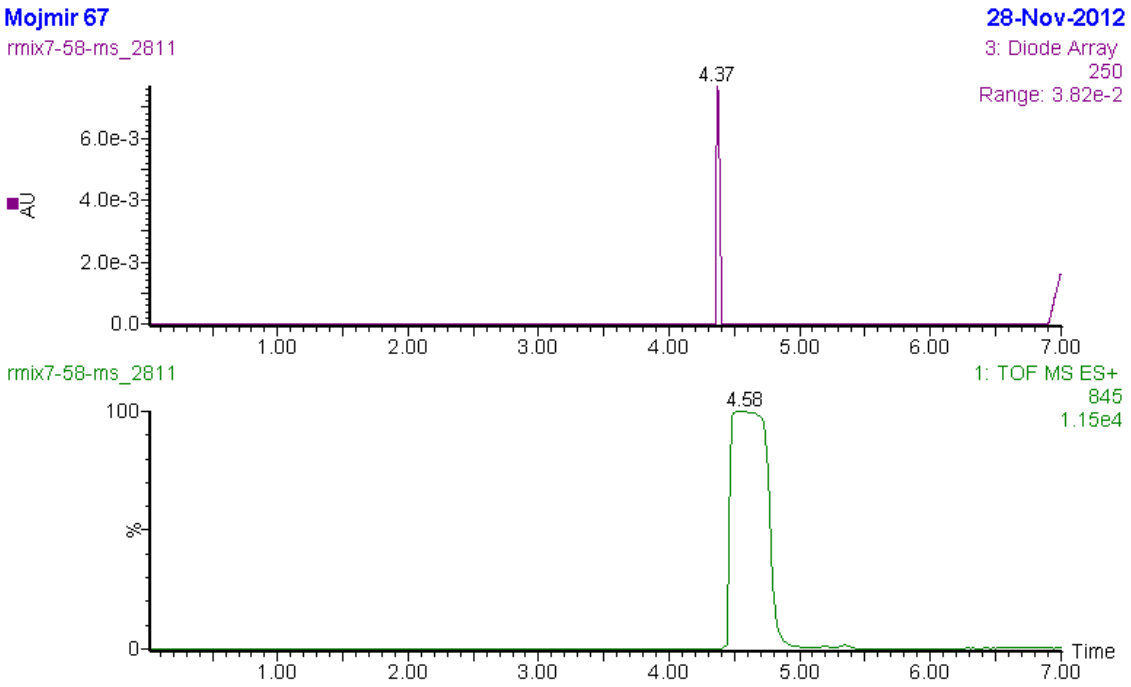

Figure S22: UPLC chromatograms (Method B) of compound **6a**, MS detector (bottom), UV detector (top).

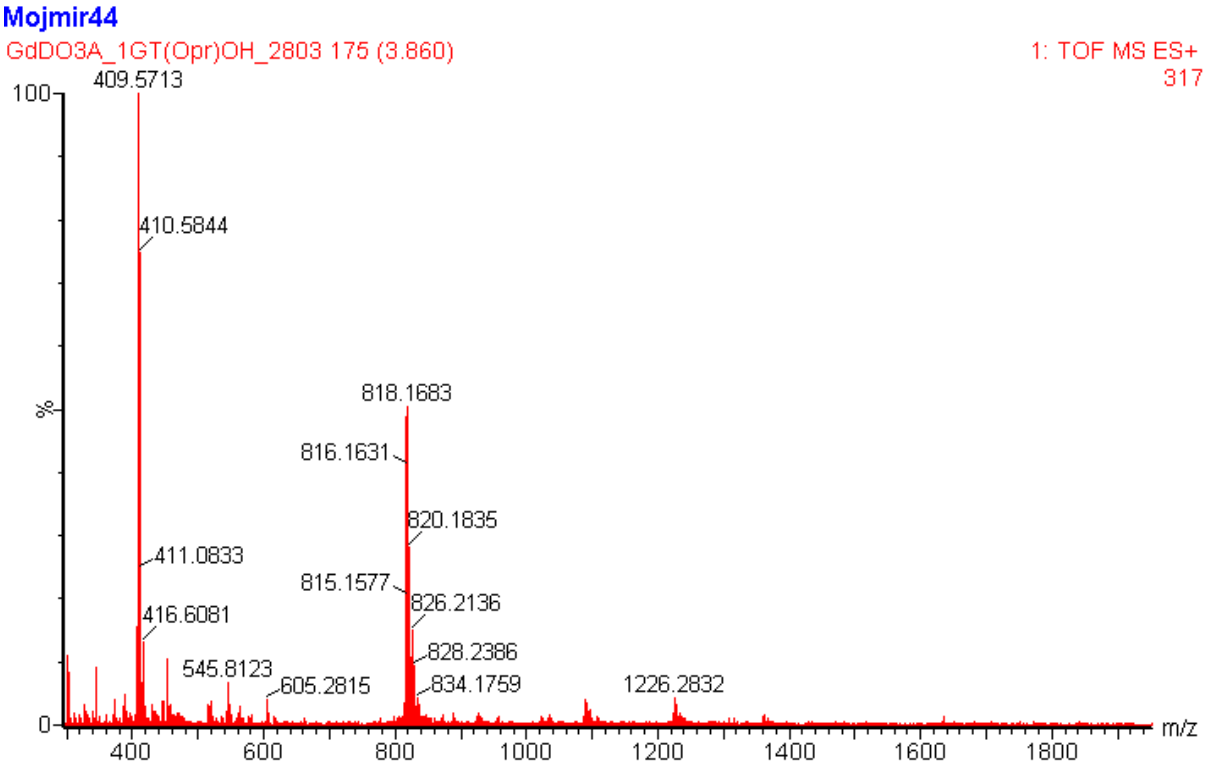

Figure S23: HR-ESI-MS spectrum of compound **6b** showing a proper charge state envelope.

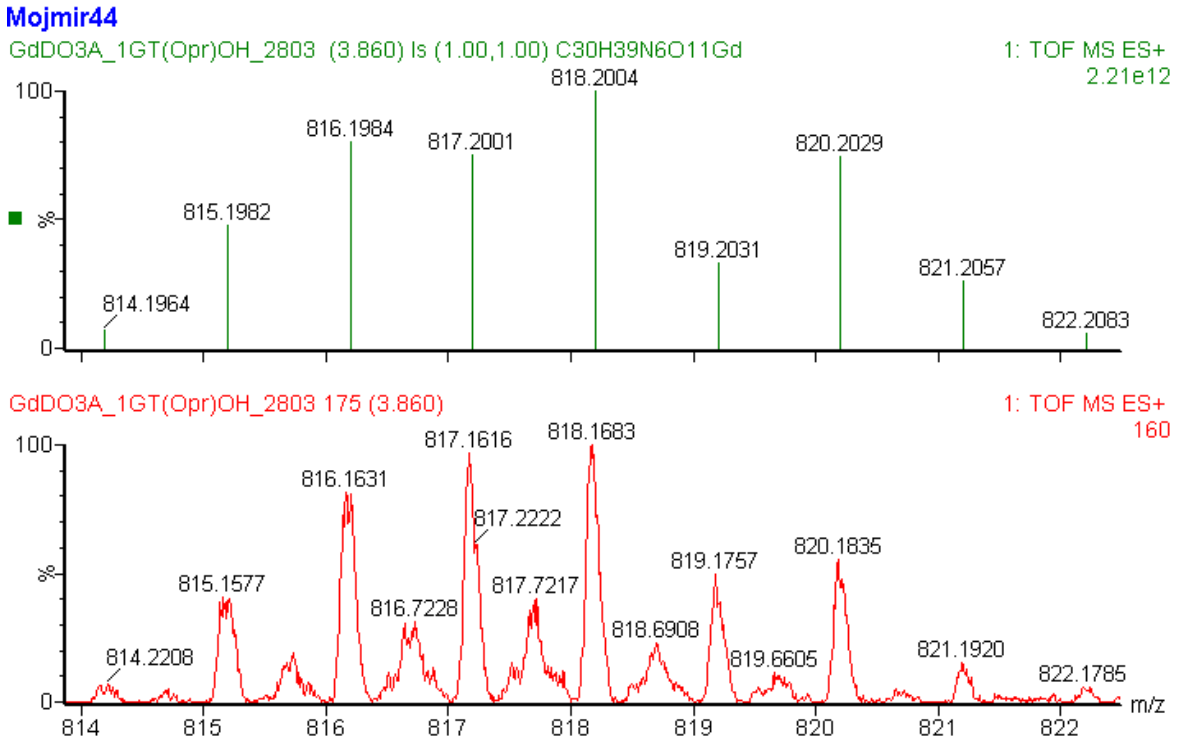

Figure S24: HR-ESI-MS spectrum of compound **6b**, M^{+} charge state observed (bottom) spectrum and calculated (top) spectrum, note the isotope pattern due to the presence of Gd.

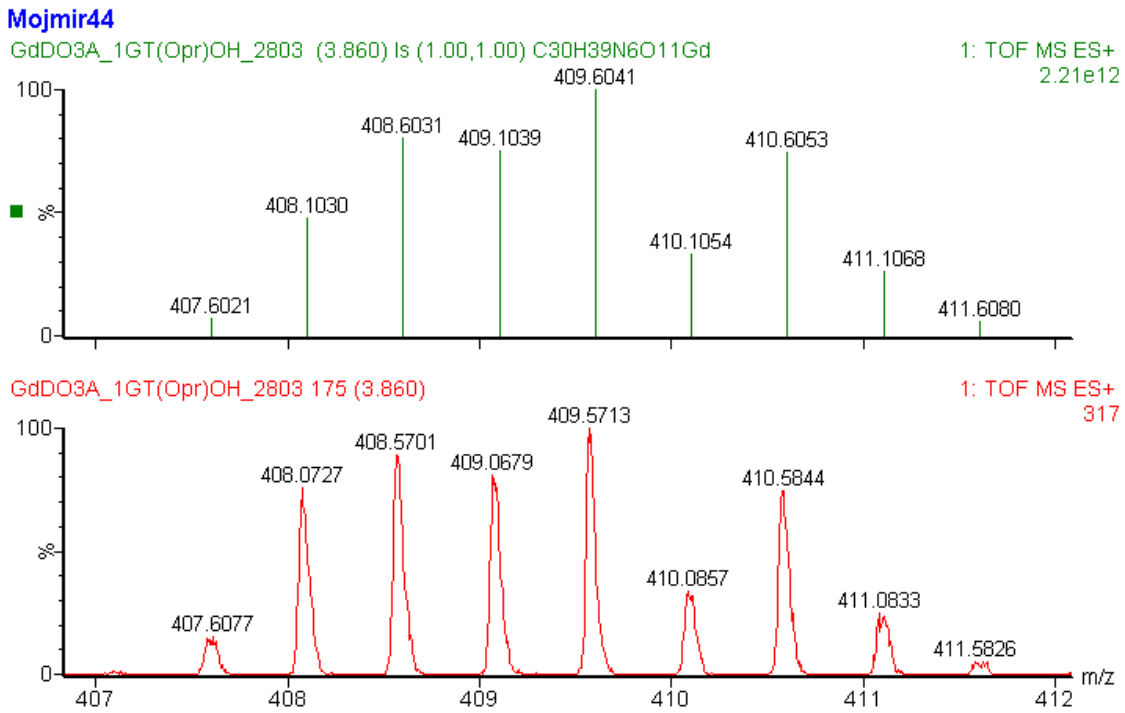

Figure S25: HR-ESI-MS spectrum of compound **6b**, M^{2+} charge state observed (bottom) spectrum and calculated (top) spectrum, note the isotope pattern due to the presence of Gd.

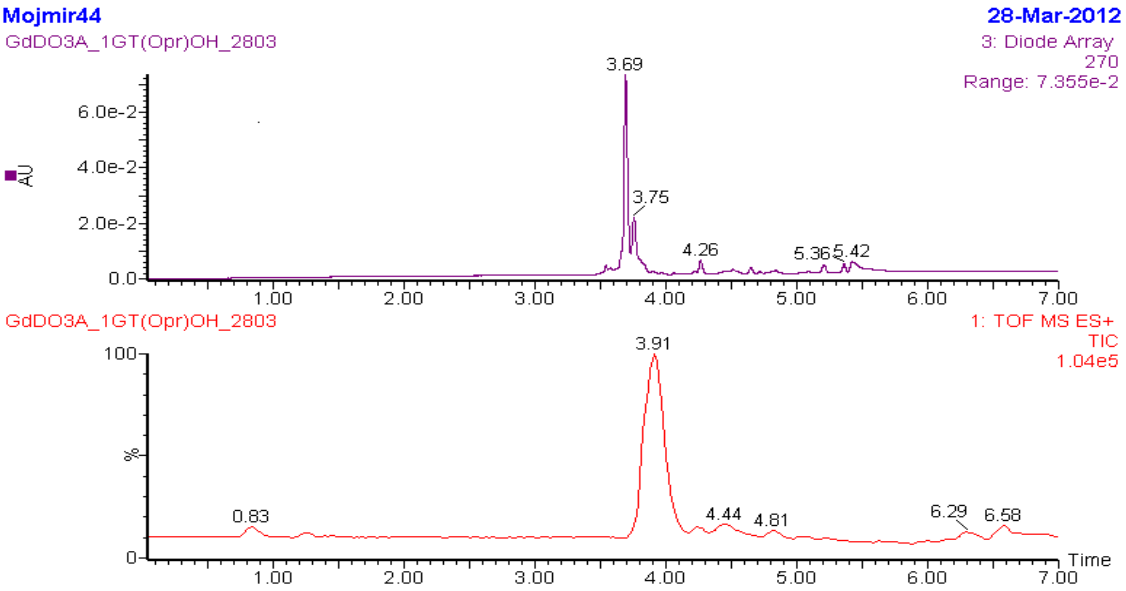

Figure S26: UPLC chromatograms (Method B) of compound **6b**, MS detector (bottom), UV detector (top).

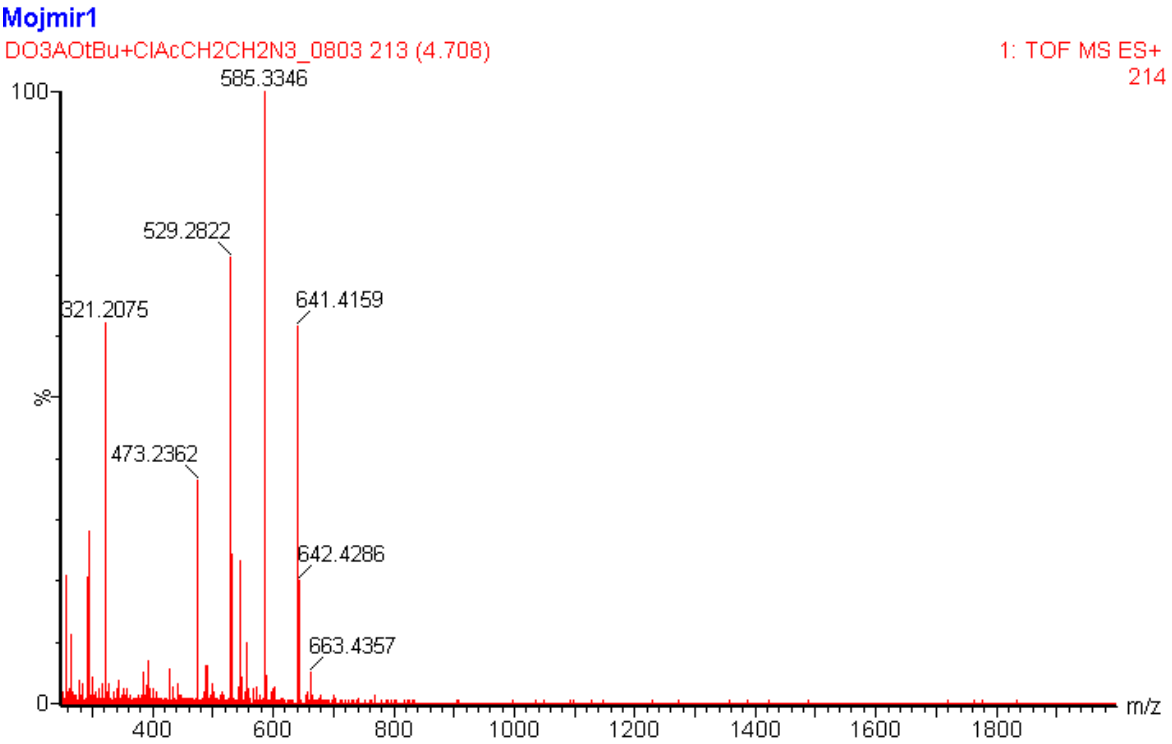

Figure S27: HR-ESI-MS spectrum of compound **7a** showing a proper charge state envelope. The *t*-Bu ester functionalities present in **7a** are not stable under the conditions of the analysis therefore M^+-56, M^+-112 and M^+-168 ions are observed for the singly charged species and M^+-28, M^+-56 and M^+-84 ions are observed for the doubly charged species.

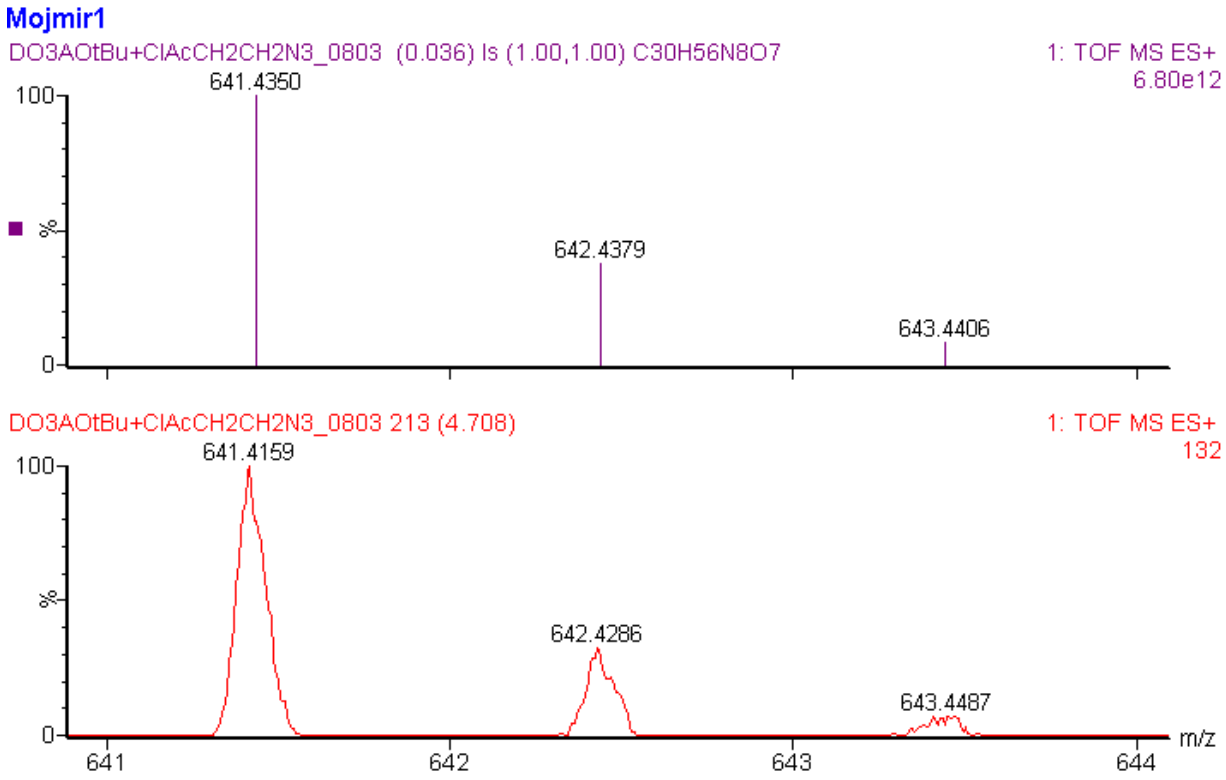

Figure S28: HR-ESI-MS spectrum of compound **7a**, M^+ charge state observed (bottom) spectrum and calculated (top) spectrum.

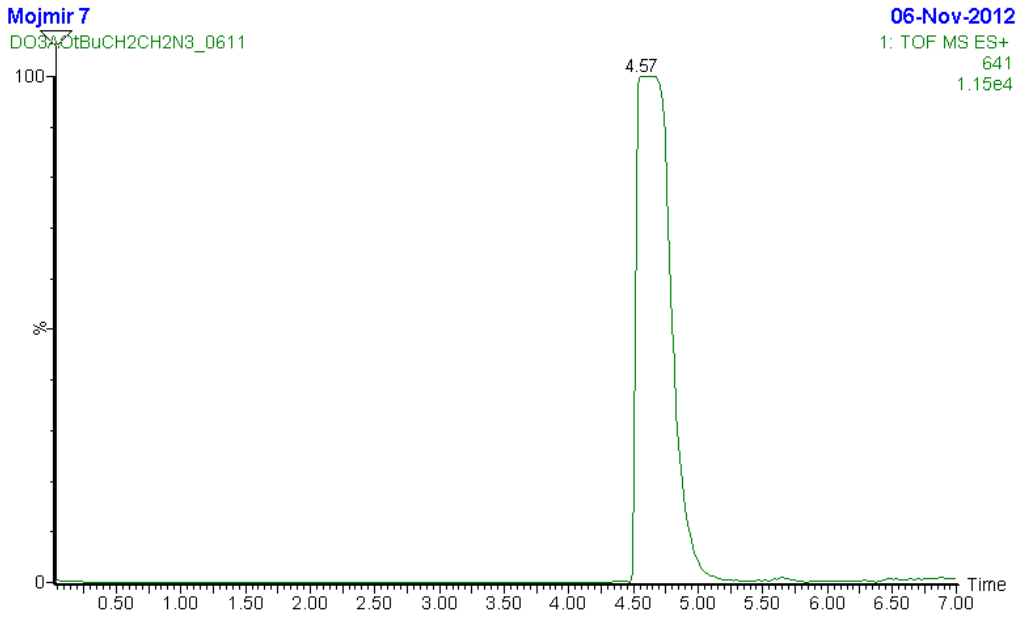

Figure S29: UPLC chromatogram (Method B) of compound **7a**, MS detector. Compound **7a** does not contain a suitable chromophore to allow for the UV detection.

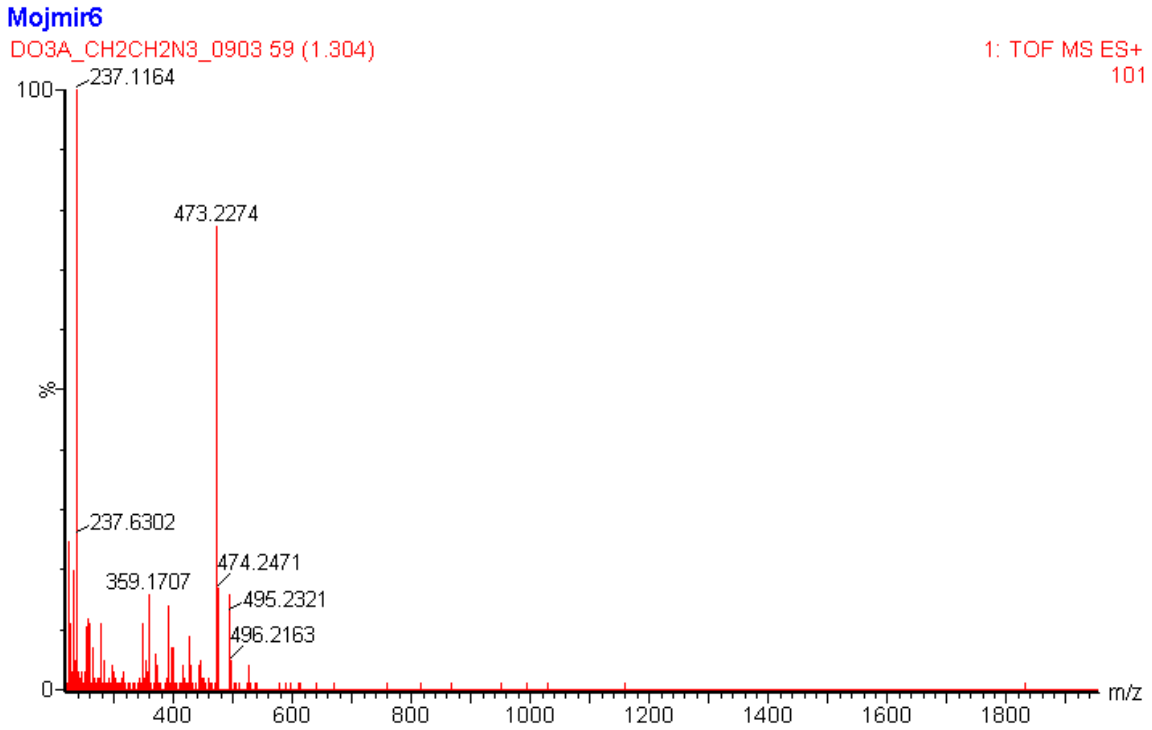

Figure S30: HR-ESI-MS spectrum of the ester deprotected version of compound **7a** showing a proper charge state envelope.

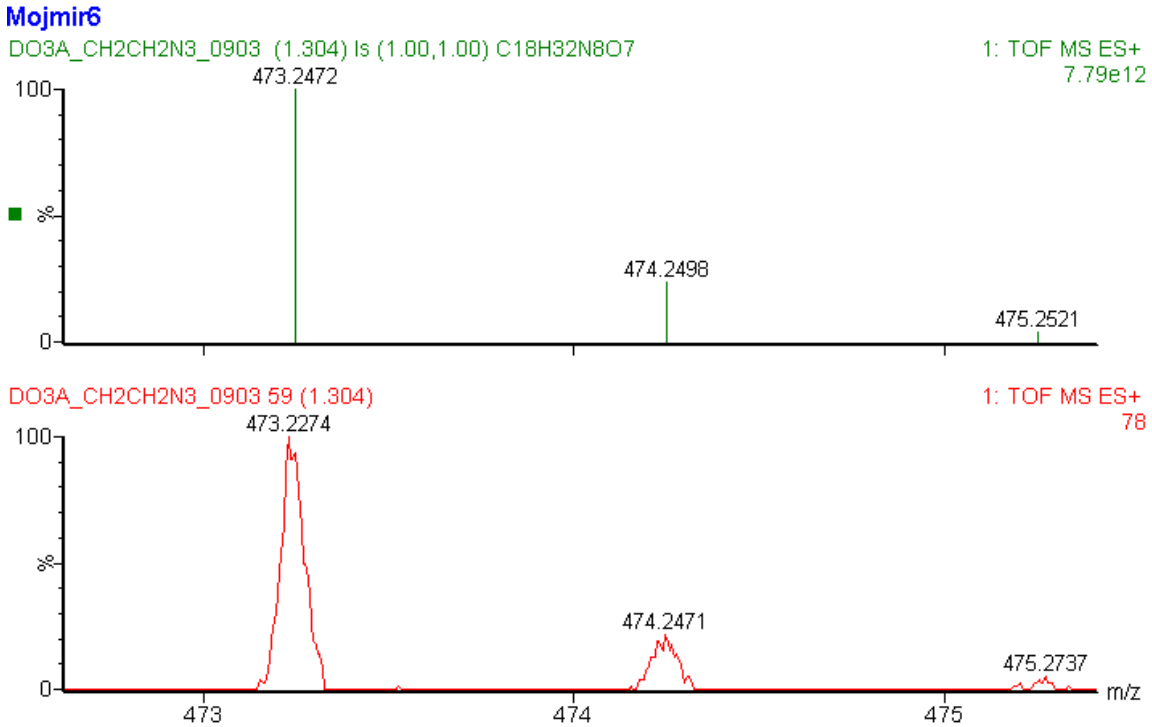

Figure S31: HR-ESI-MS spectrum of the ester deprotected version of compound **7a**, M^+ charge state observed (bottom) spectrum and calculated (top) spectrum.

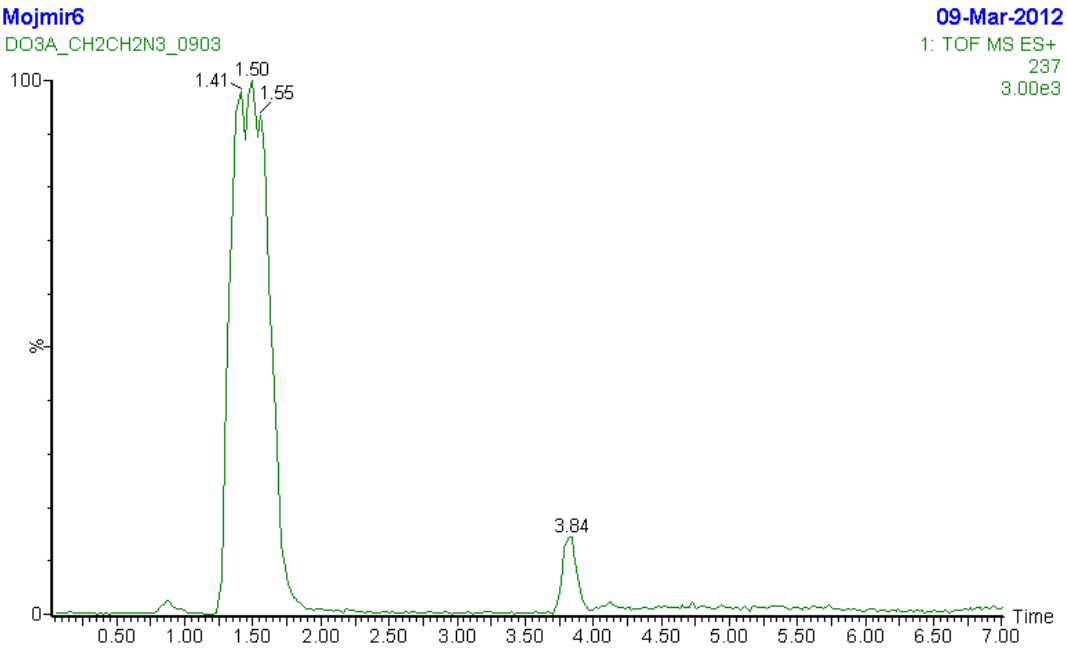

Figure S32: UPLC chromatogram (Method B) of the ester deprotected version of compound **7a**, MS detector. Compound does not contain a suitable chromophore to allow for the UV detection.

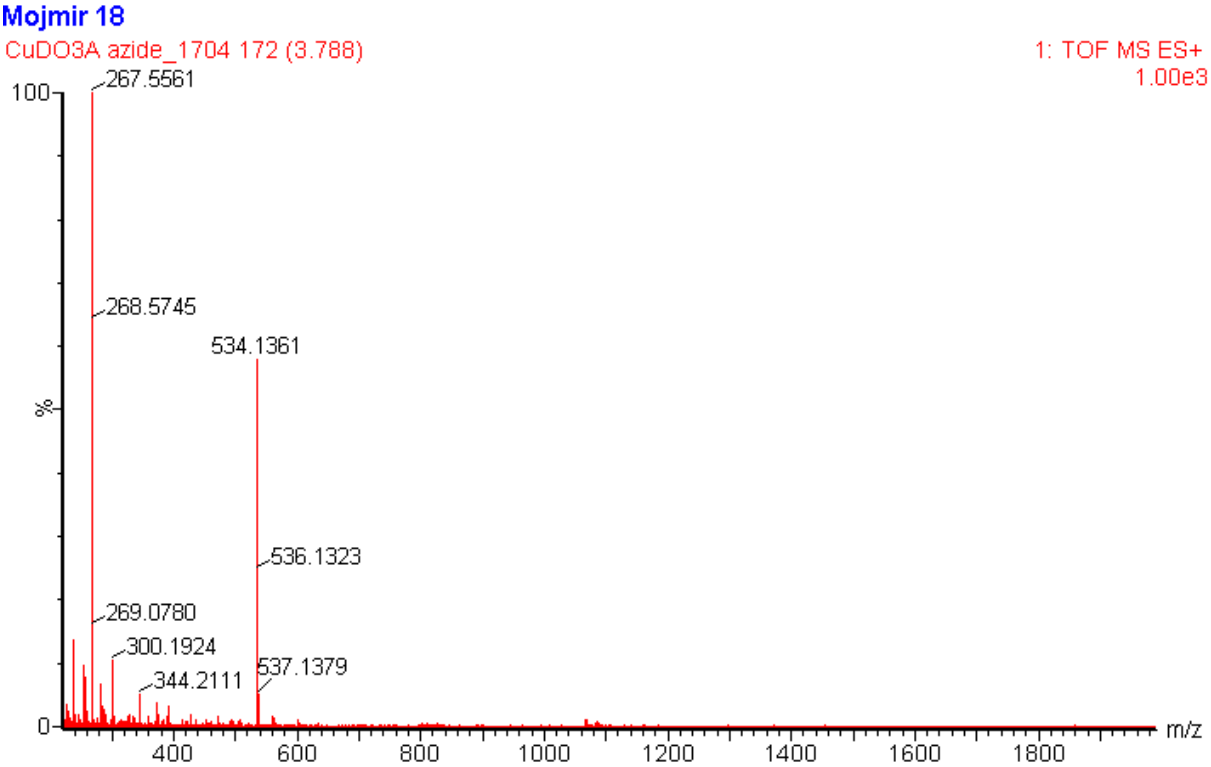

Figure S33: HR-ESI-MS spectrum of compound **7b** showing a proper charge state envelope.

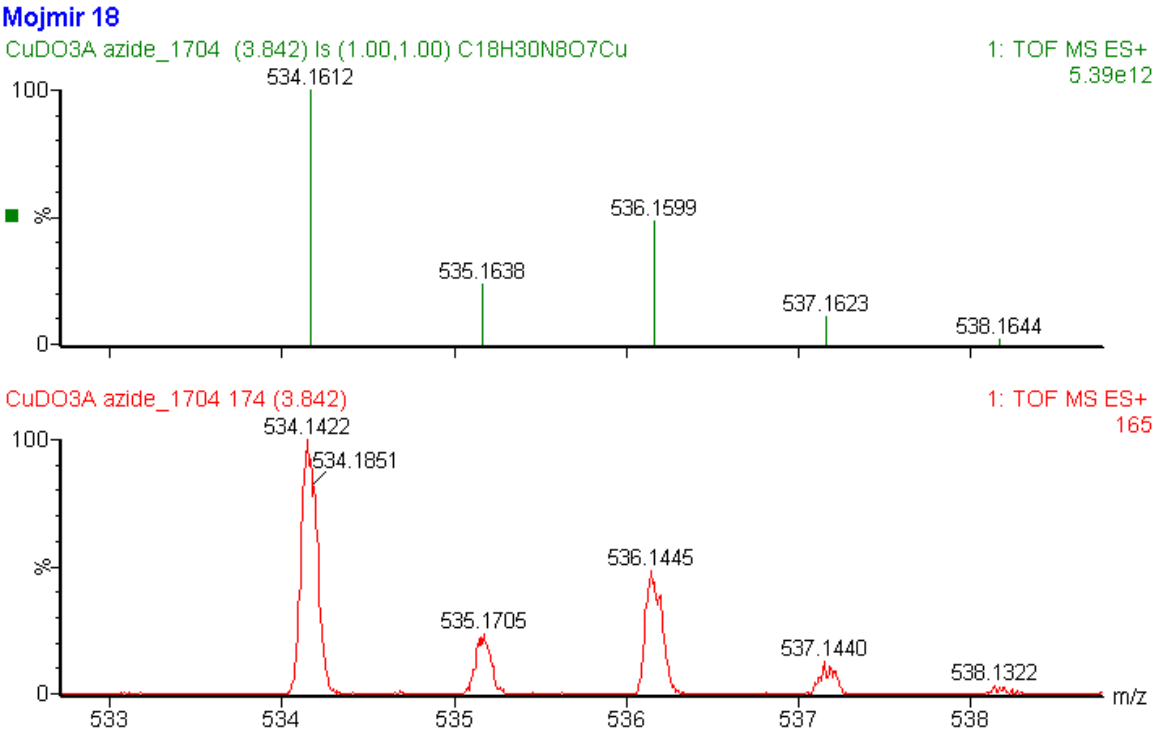

Figure S34: HR-ESI-MS spectrum of compound **7b**, M^{+} charge state observed (bottom) spectrum and calculated (top) spectrum, note the isotope pattern due to the presence of Cu.

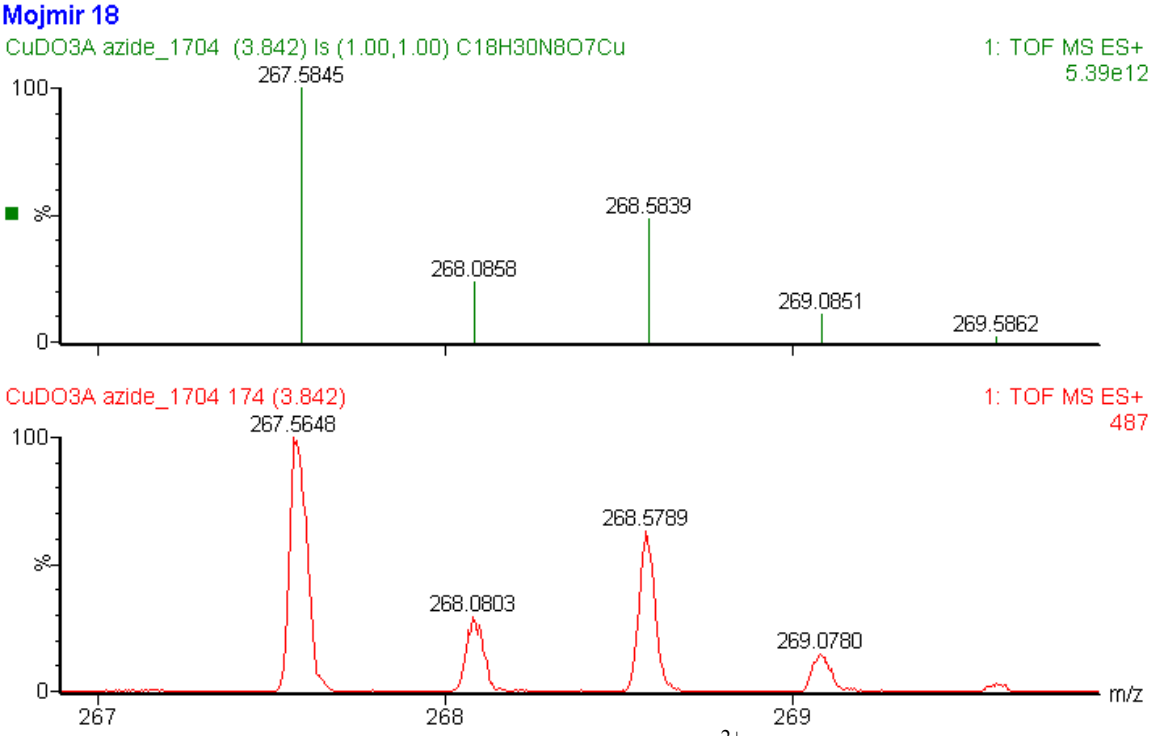

Figure S35: HR-ESI-MS spectrum of compound **7b**, M^{2+} charge state observed (bottom) spectrum and calculated (top) spectrum, note the isotope pattern due to the presence of Cu.

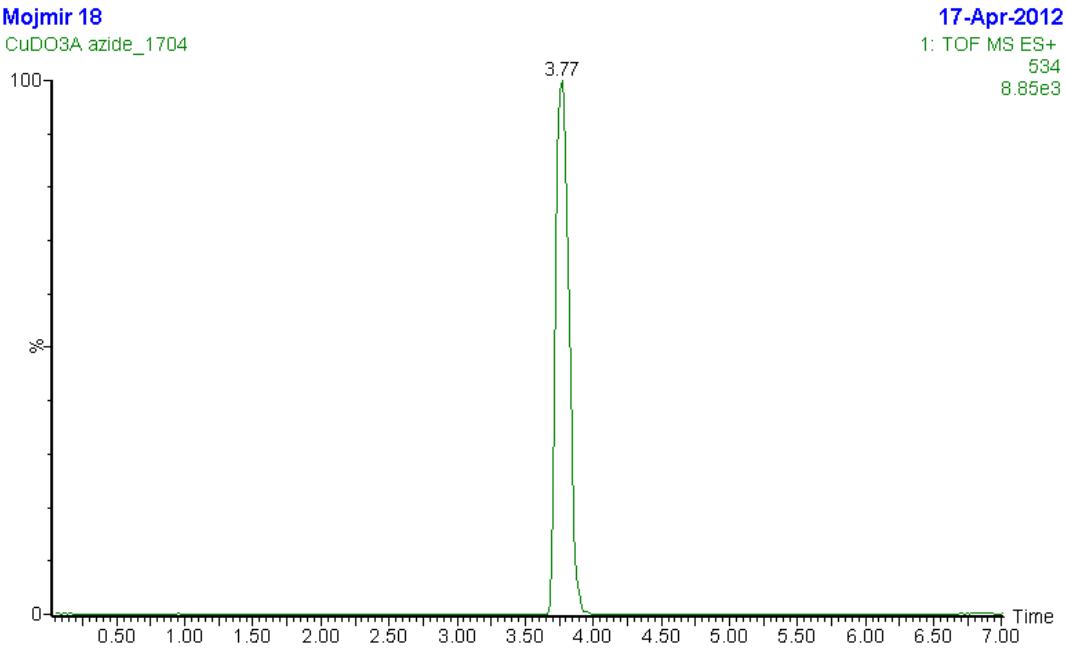

Figure S36: UPLC chromatogram (Method B) of compound **7b**, MS detector. Compound **7b** does not contain a suitable chromophore to allow for the UV detection.

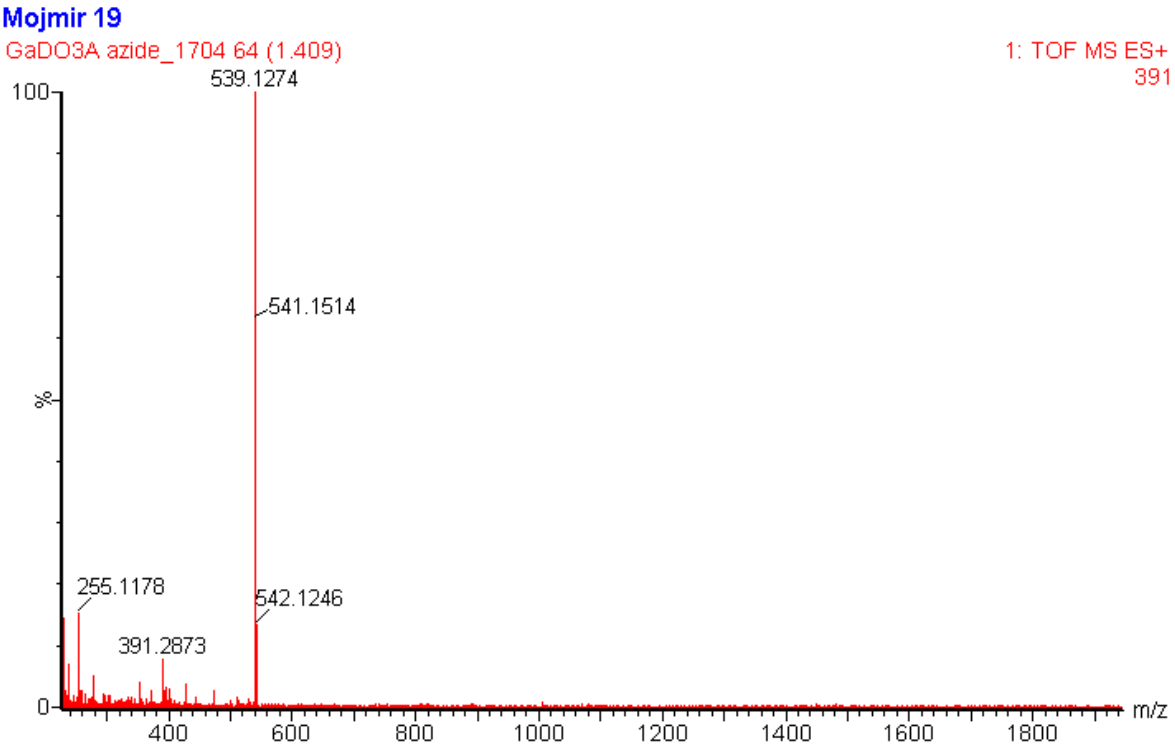

Figure S37: HR-ESI-MS spectrum of compound **7c**.

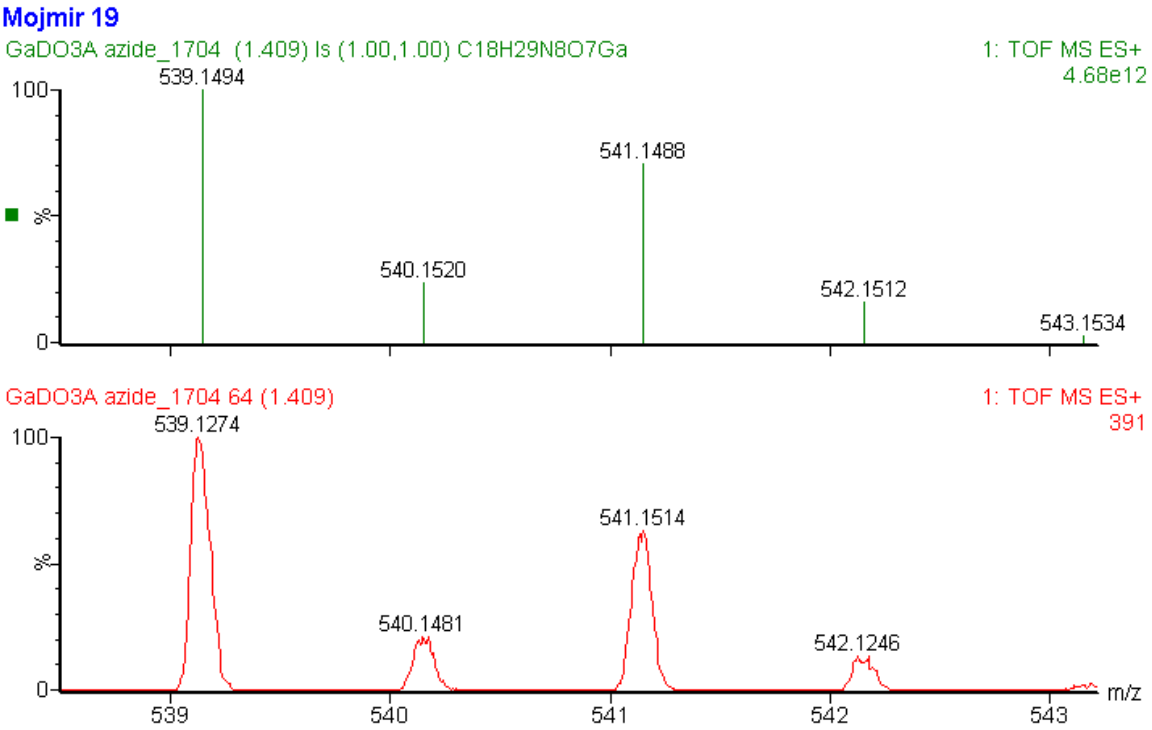

Figure S38: HR-ESI-MS spectrum of compound **7c**, M^+ charge state observed (bottom) spectrum and calculated (top) spectrum, note the isotope pattern due to the presence of Ga.

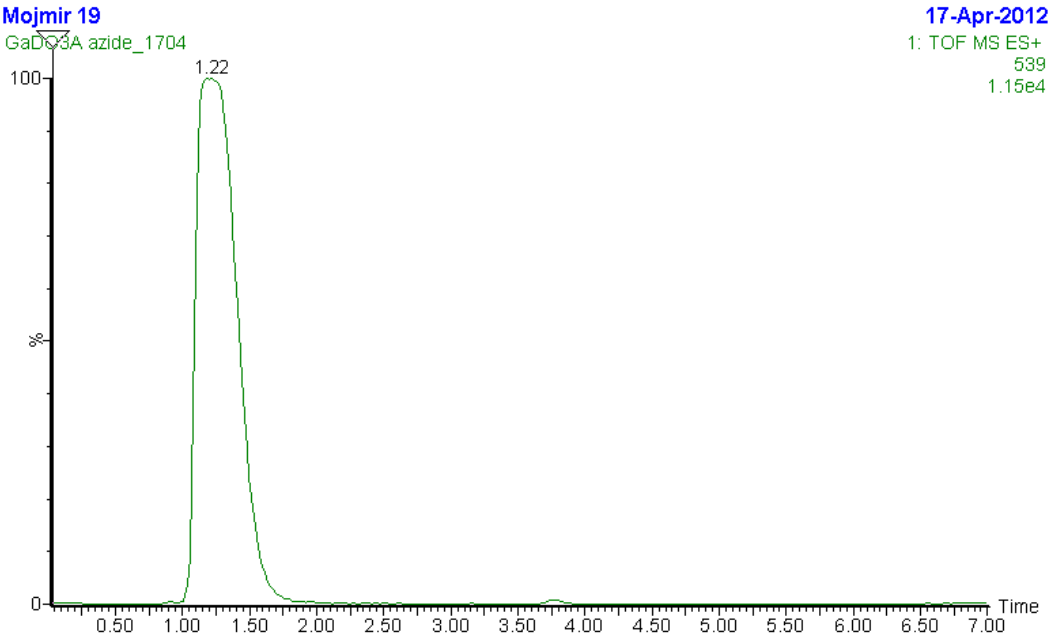

Figure S39: UPLC chromatogram (Method B) of compound **7c**, MS detector. Compound **7c** does not contain a suitable chromophore to allow for the UV detection.

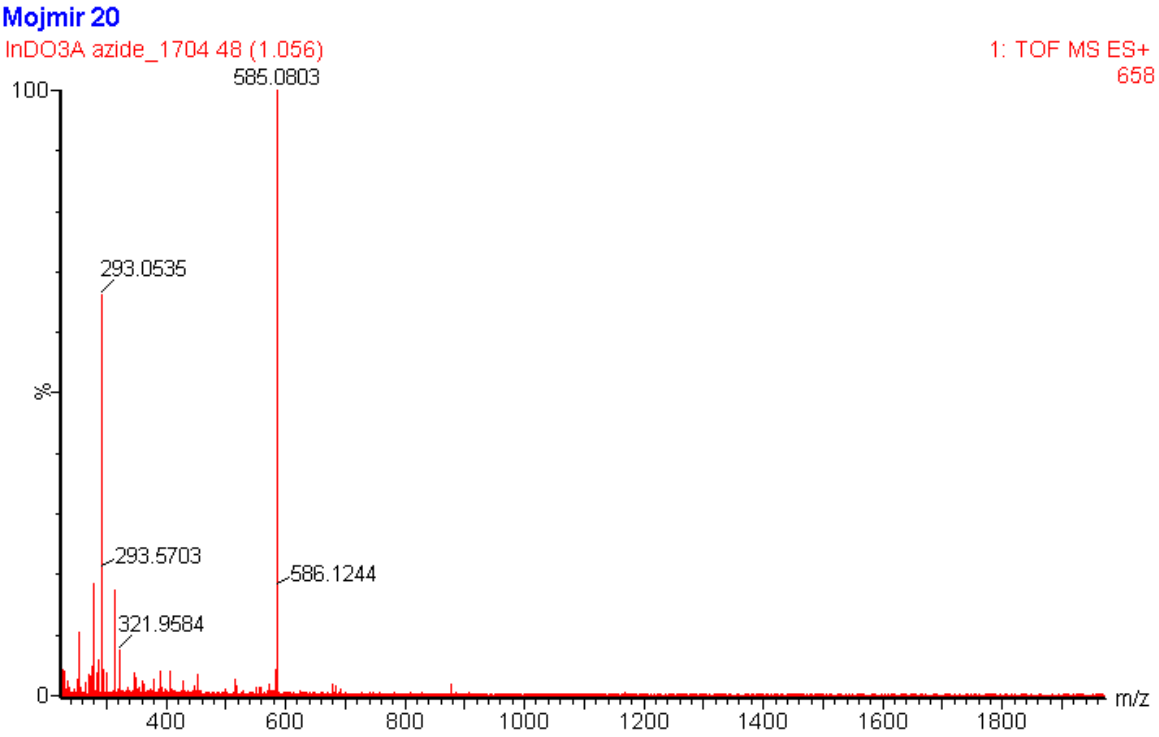

Figure S40: HR-ESI-MS spectrum of compound **7d** showing a proper charge state envelope.

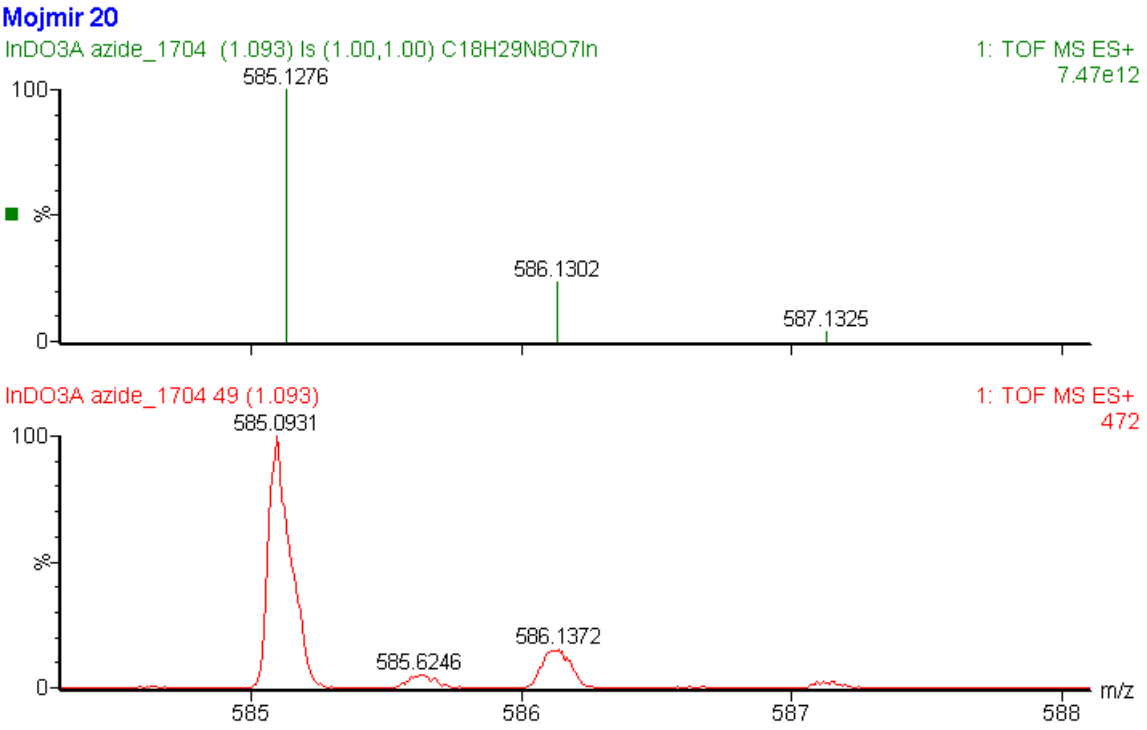

Figure S41: HR-ESI-MS spectrum of compound **7d**, M^+ charge state observed (bottom) spectrum and calculated (top) spectrum, note that In only possesses one stable isotope.

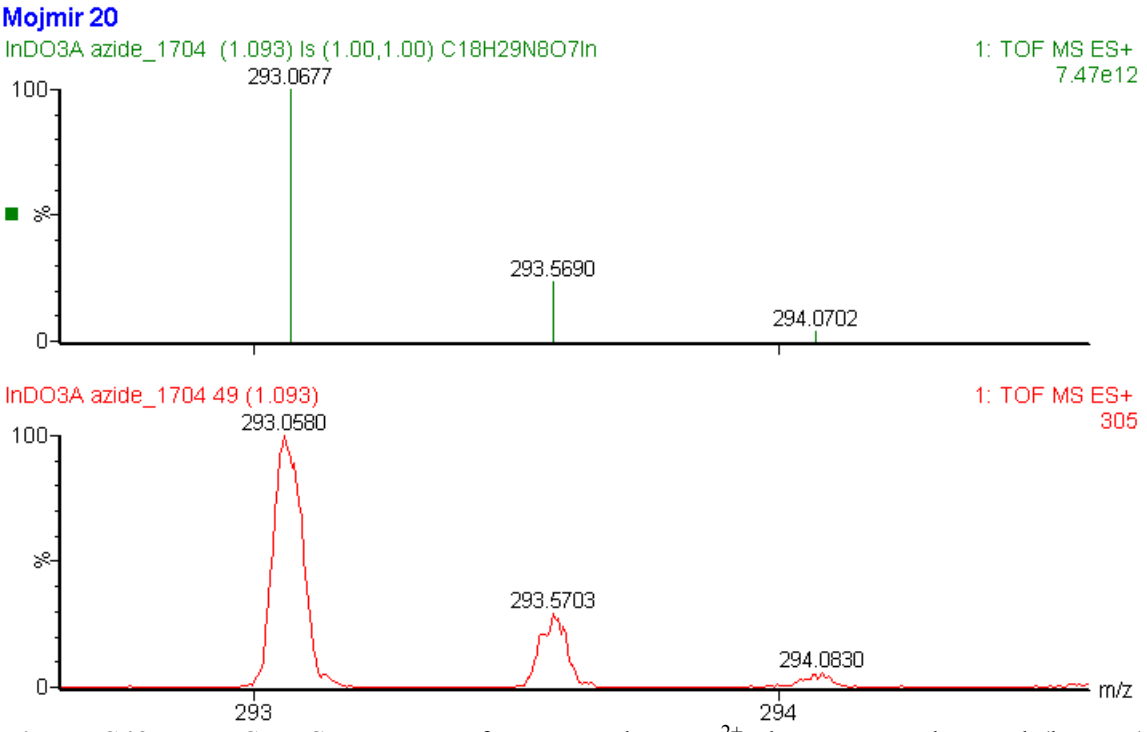

Figure S42: HR-ESI-MS spectrum of compound **7d**, M^{2+} charge state observed (bottom) spectrum and calculated (top) spectrum, note that In only possesses one stable isotope.

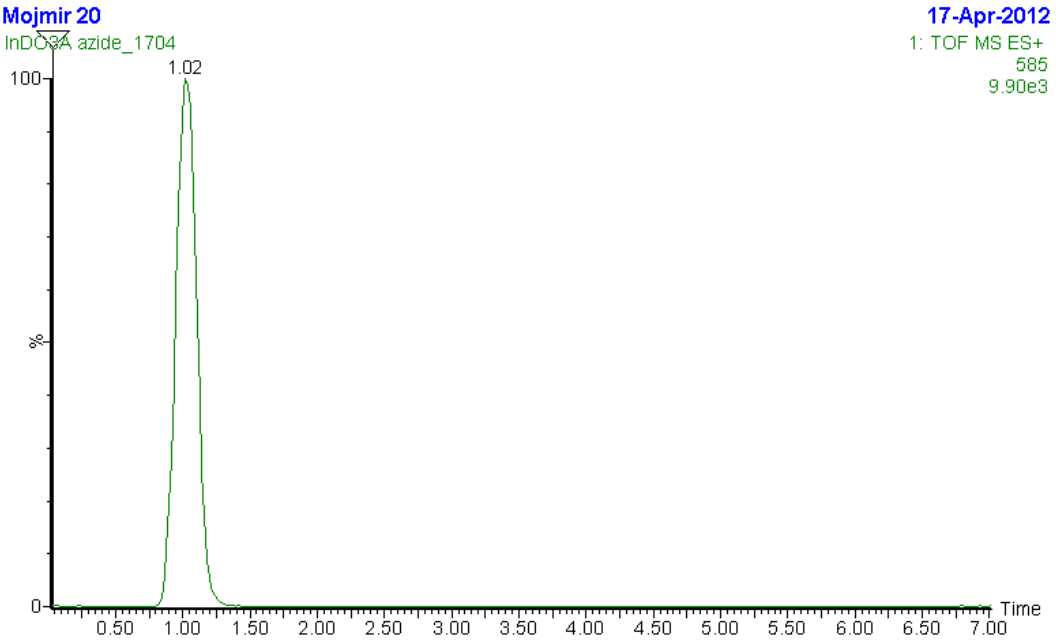

Figure S43: UPLC chromatogram (Method B) of compound **7d**, MS detector. Compound **7d** does not contain a suitable chromophore to allow for the UV detection.

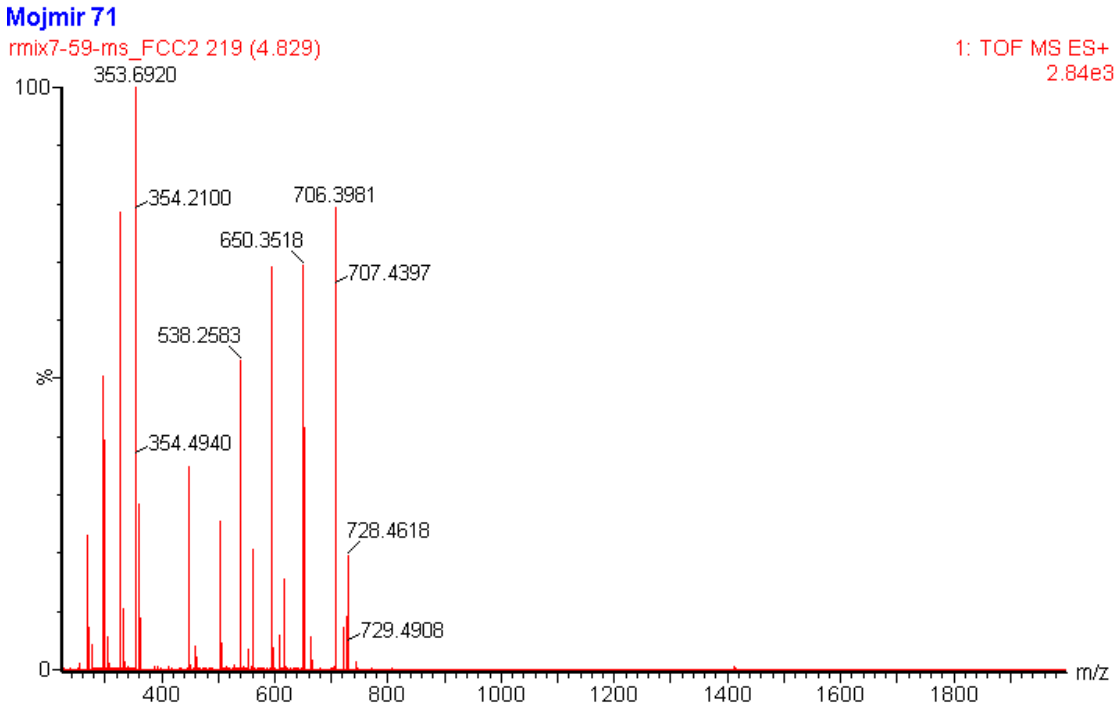

Figure S44: HR-ESI-MS spectrum of compound **13** showing a proper charge state envelope. The *t*-Bu ester functionalities present in **13** are not stable under the conditions of the analysis therefore M^+-56, M^+-112 and M^+-168 ions are observed for the singly charged species and M^+-28, M^+-56 and M^+-84 ions are observed for the doubly charged species.

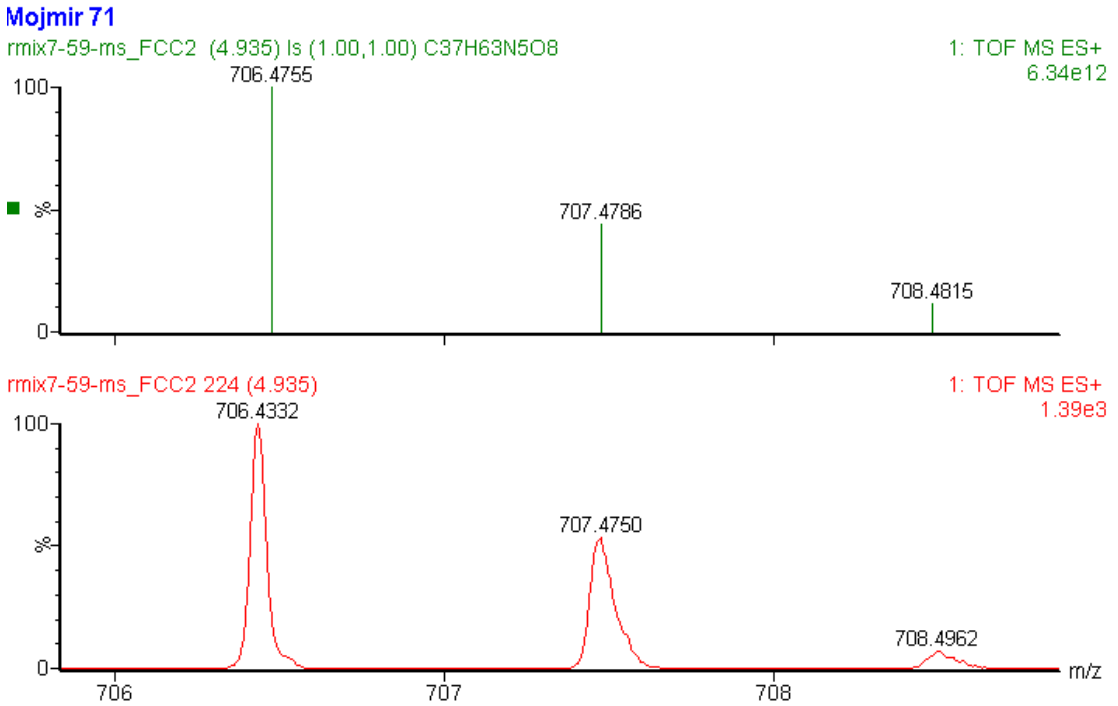

Figure S45: HR-ESI-MS spectrum of compound **13**, M^+ charge state observed (bottom) spectrum and calculated (top) spectrum.

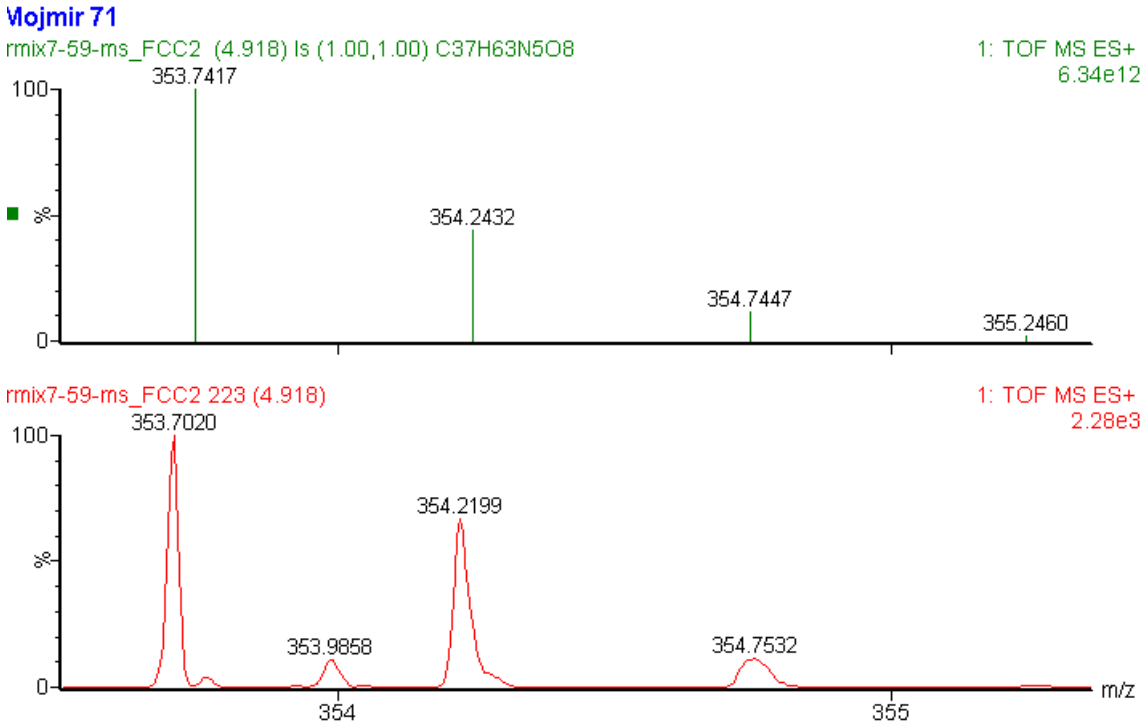

Figure S46: HR-ESI-MS spectrum of compound **13**, M^{2+} charge state observed (bottom) spectrum and calculated (top) spectrum.

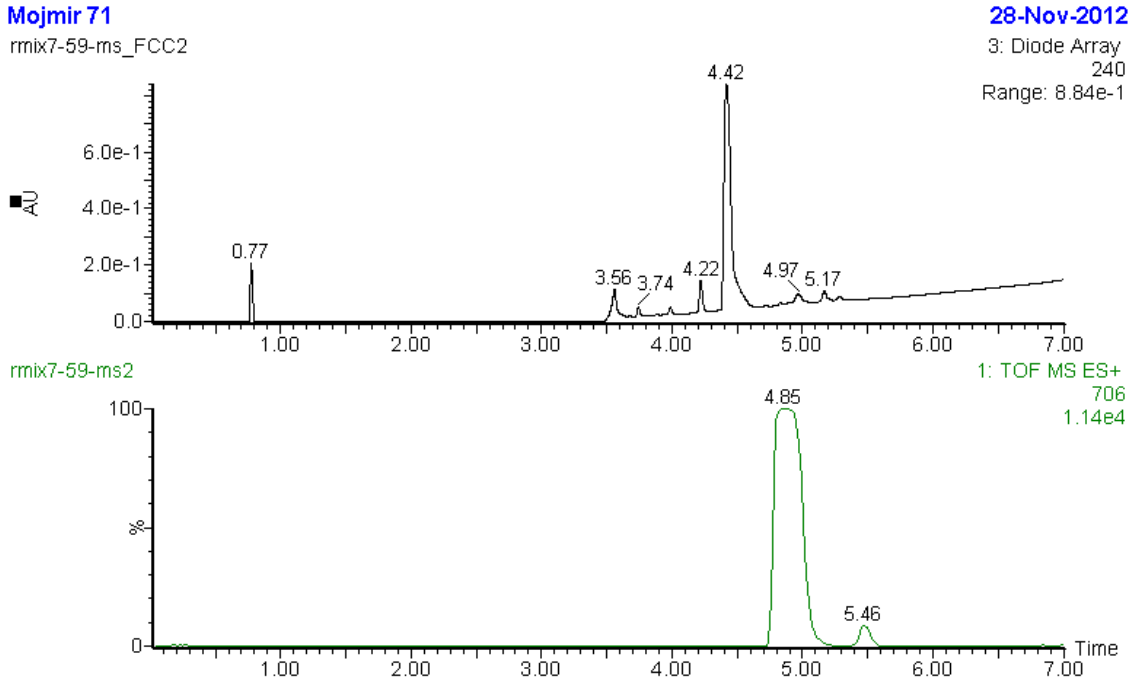

Figure S47: UPLC chromatograms (Method B) of compound **13**, MS detector (bottom), UV detector (top).

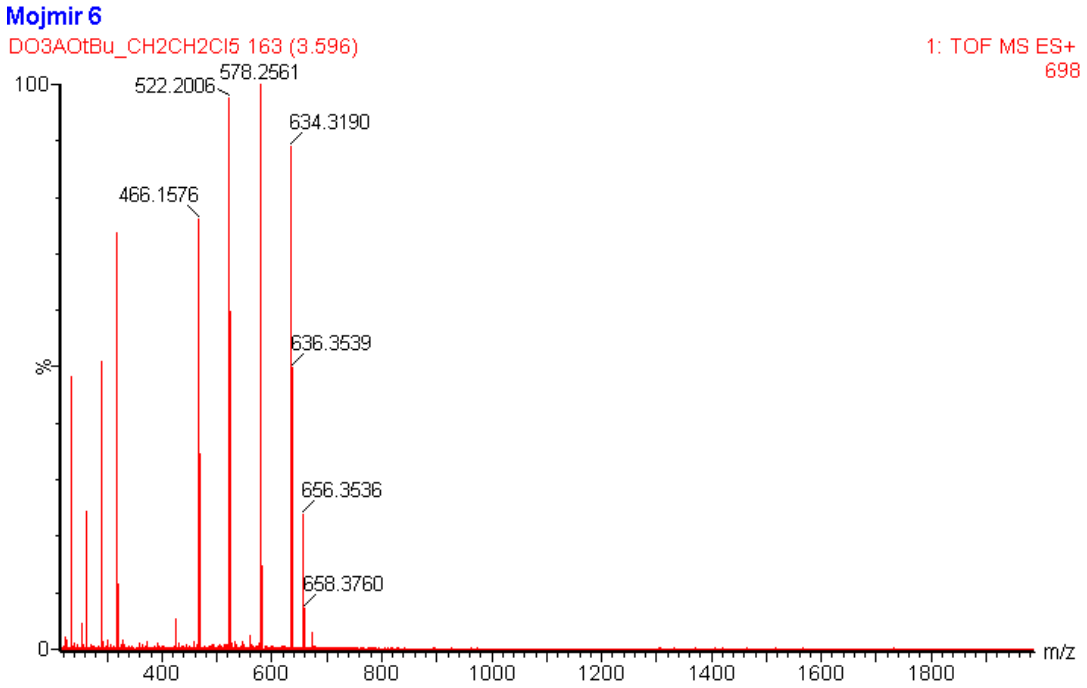

Figure S48: HR-ESI-MS spectrum of DO3A-*Ot*Bu-Ac 2-chloroethylamine showing a proper charge state envelope. The *t*-Bu ester functionalities present in this intermediate are not stable under the conditions of the analysis therefore M^+-56, M^+-112 and M^+-168 ions are observed for the singly charged species and M^+-28, M^+-56 and M^+-84 ions are observed for the doubly charged species.

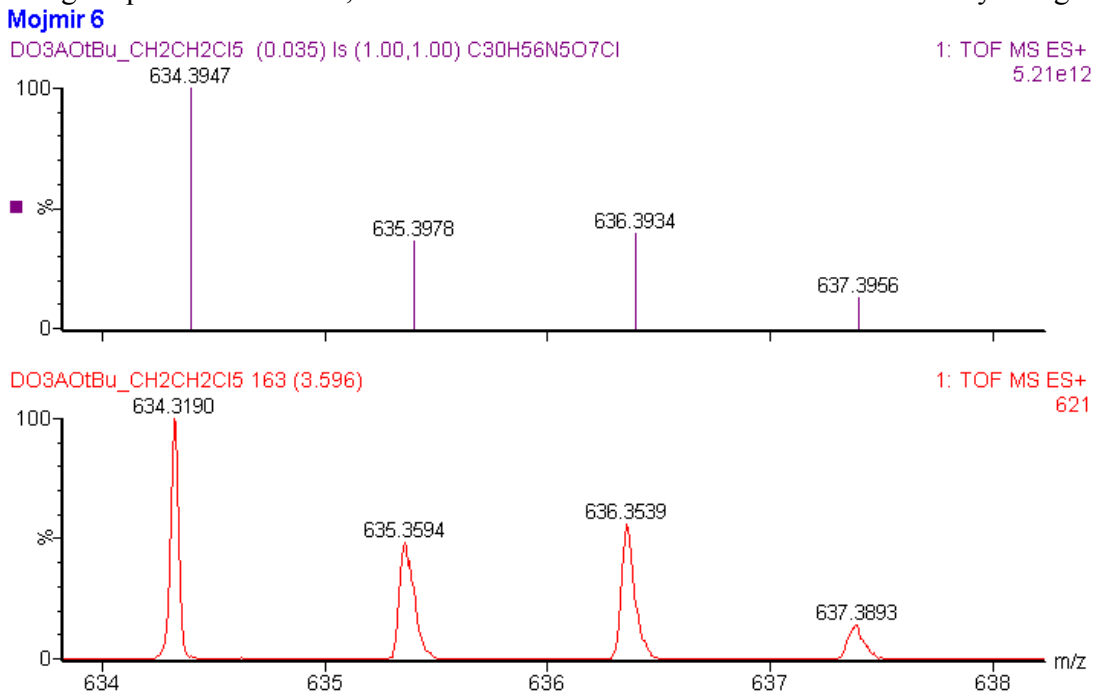

Figure S49: HR-ESI-MS spectrum of DO3A-*Ot*Bu-Ac 2-chloroethylamine, M^+ charge state observed (bottom) spectrum and calculated (top) spectrum, note the isotope pattern due to the presence of Cl.

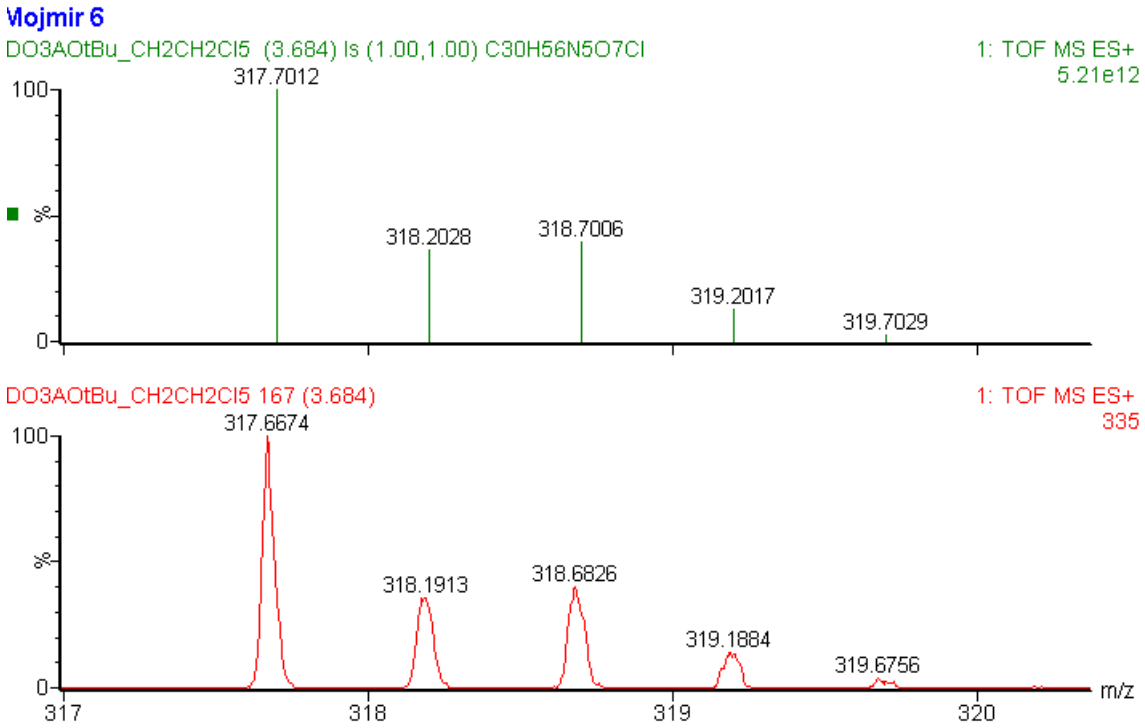

Figure S50: HR-ESI-MS spectrum of DO3A-*Ot*Bu-Ac 2-chloroethylamine, M^{2+} charge state observed (bottom) spectrum and calculated (top) spectrum, note the isotope pattern due to the presence of Cl.

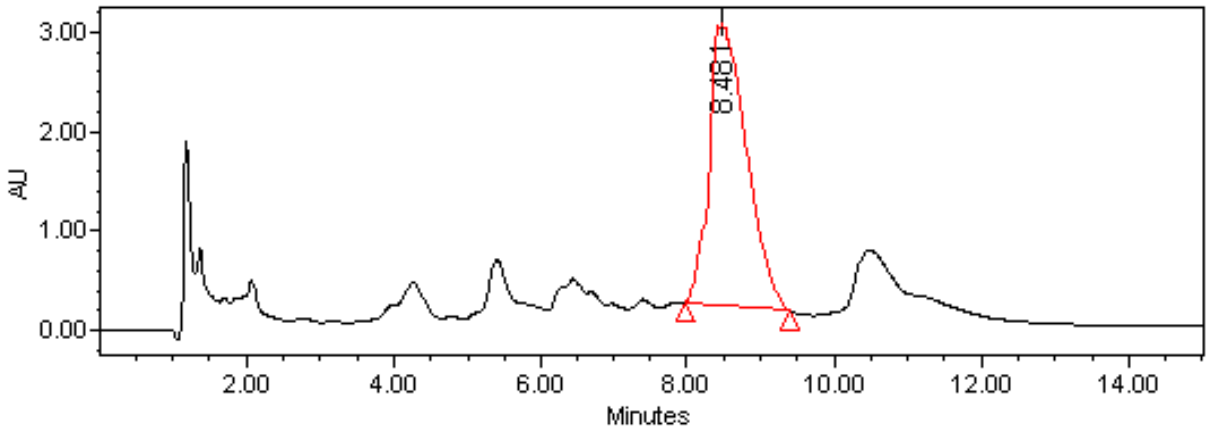

Figure S51: HPLC chromatogram (Method A) obatined during the semi-preparative purification of crude reaction mixture containing the Gd^{3+}/Cu^{2+} heterometallic complex **5a** (t_R 8.5 min).

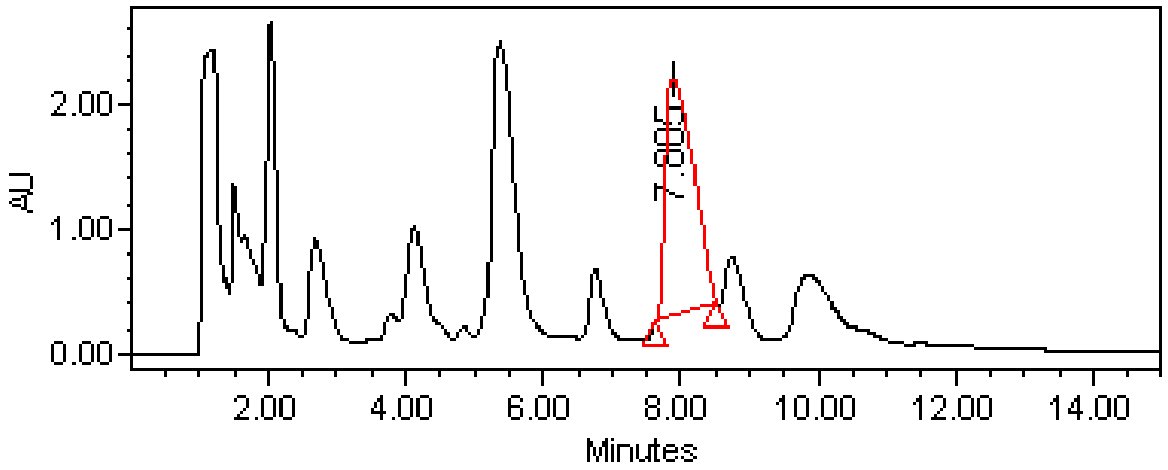

Figure S52: HPLC chromatogram (Method A) obatined during the semi-preparative purification of crude reaction mixture containing the Gd^{3+}/Ga^{3+} heterometallic complex **5b** (t_R 7.8 min).

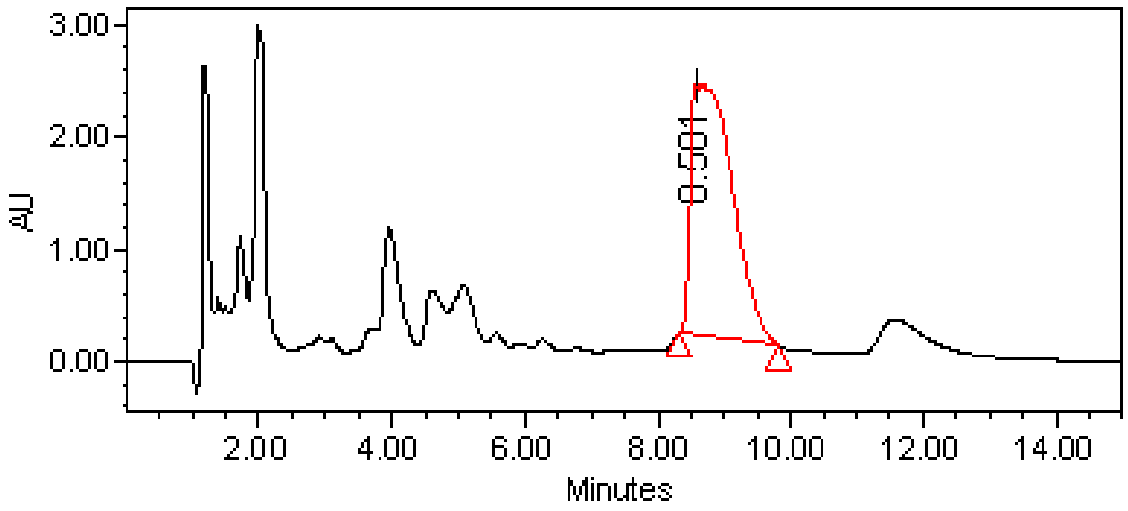

Figure S53: HPLC chromatogram (Method A) obtained during the semi-preparative purification of crude reaction mixture containing the Gd^{3+}/In^{3+} heterometallic complex **5c** (t_R 8.5 min).

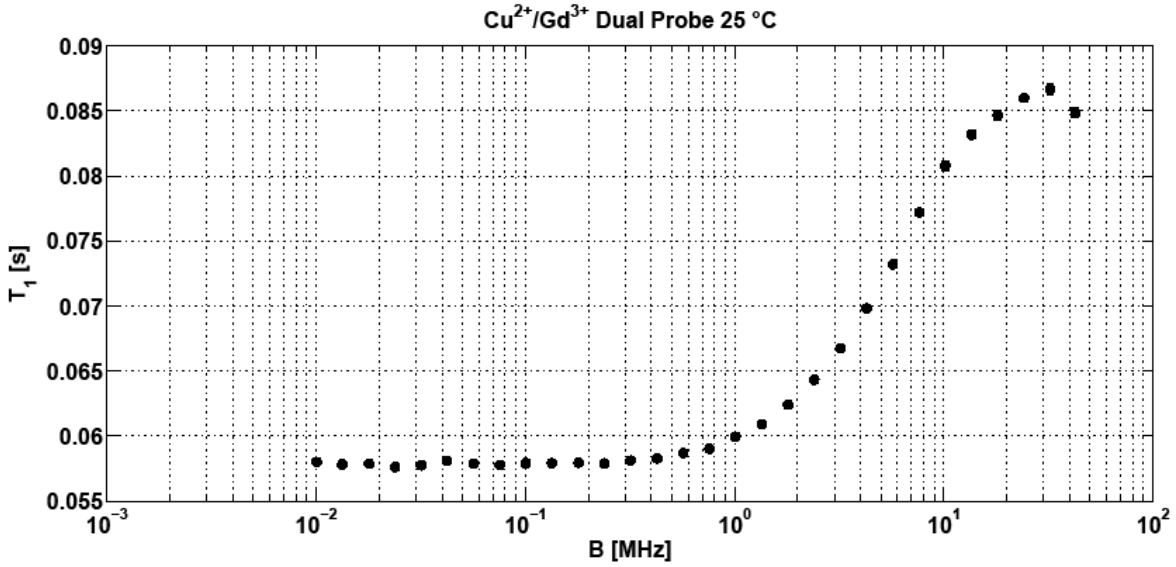

Figure S54: Dependence of T_1 relaxation time on the magnetic field strength for the Gd^{3+}/Cu^{2+} heterometallic complex **5a**, acquired at 25 °C.

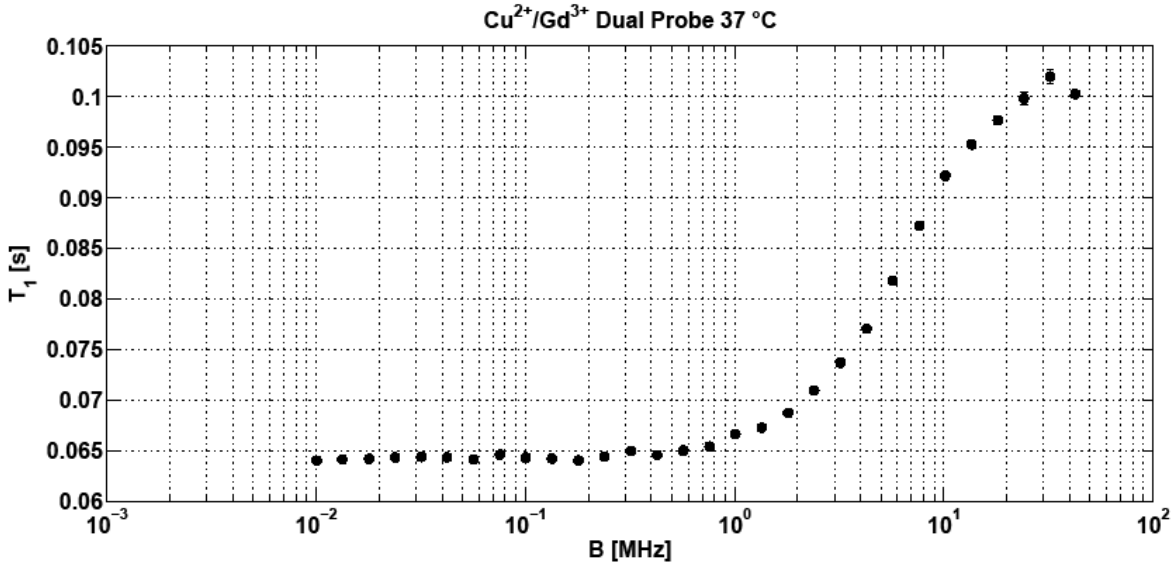

Figure S55: Dependence of T_1 relaxation time on the magnetic field strength for the Gd^{3+}/Cu^{2+} heterometallic complex **5a**, acquired at 37 °C.

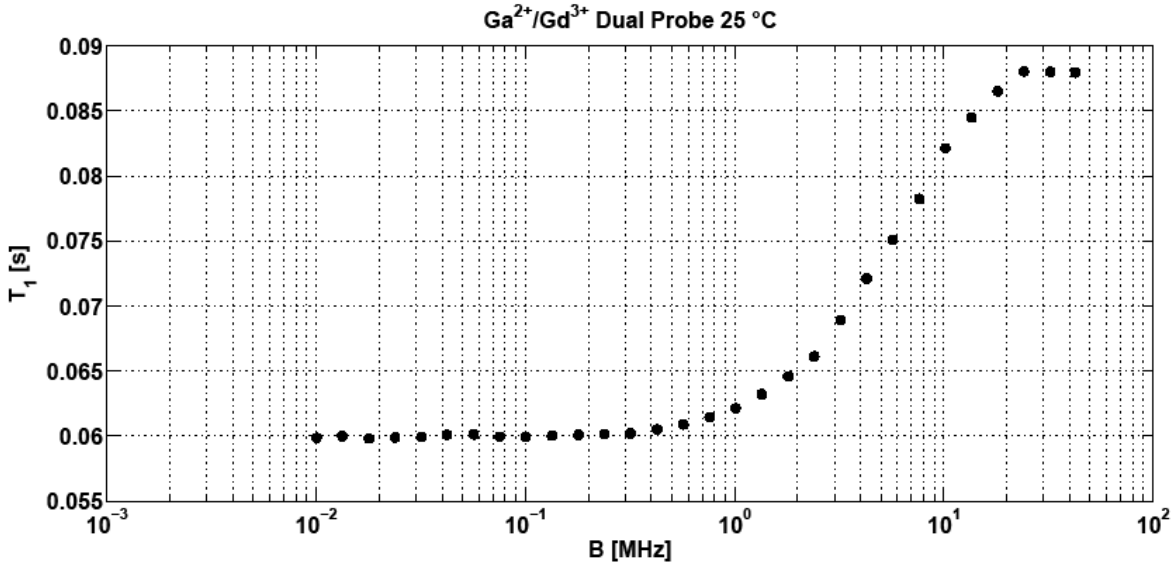

Figure S56: Dependence of T_1 relaxation time on the magnetic field strength for the Gd^{3+}/Ga^{3+} heterometallic complex **5b**, acquired at 25 °C.

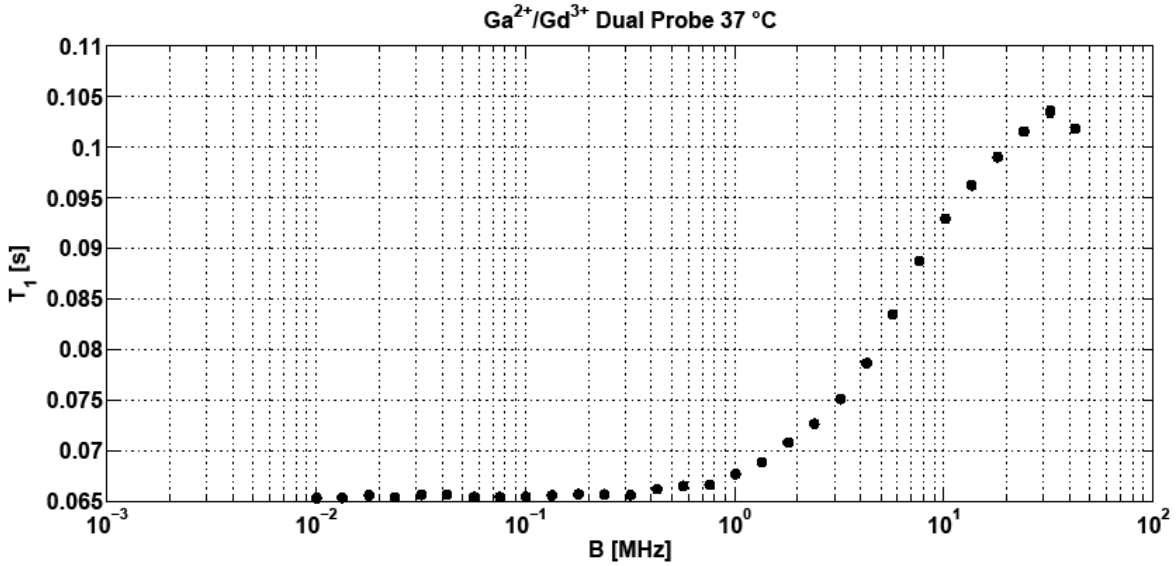

Figure S57: Dependence of T_1 relaxation time on the magnetic field strength for the Gd^{3+}/Ga^{3+} heterometallic complex **5b**, acquired at 37 °C.

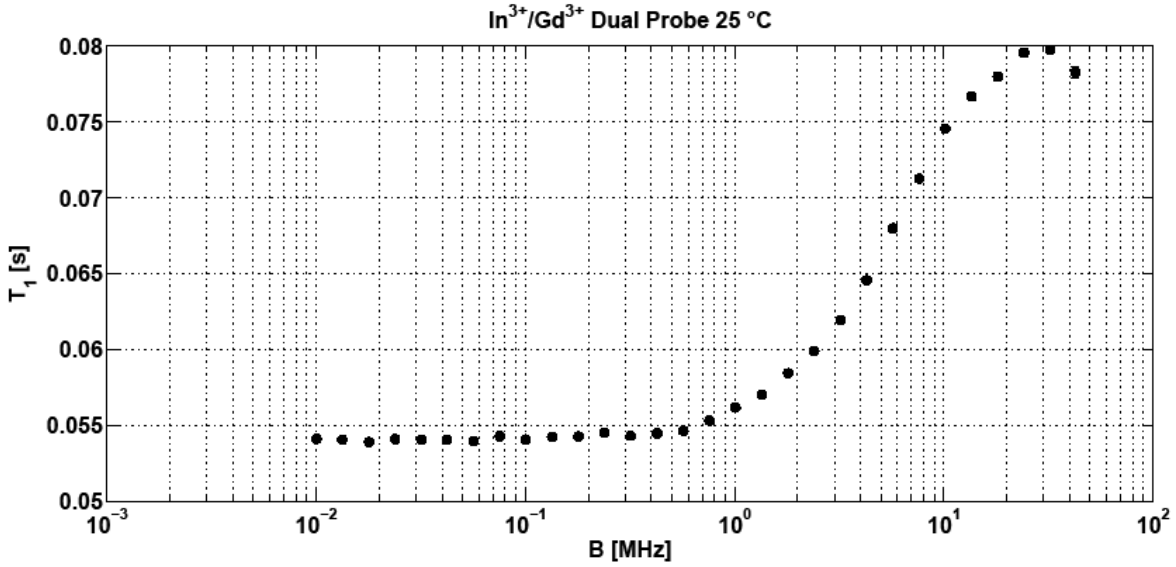

Figure S58: Dependence of T_1 relaxation time on the magnetic field strength for the Gd^{3+}/In^{3+} heterometallic complex **5c**, acquired at 25 °C.

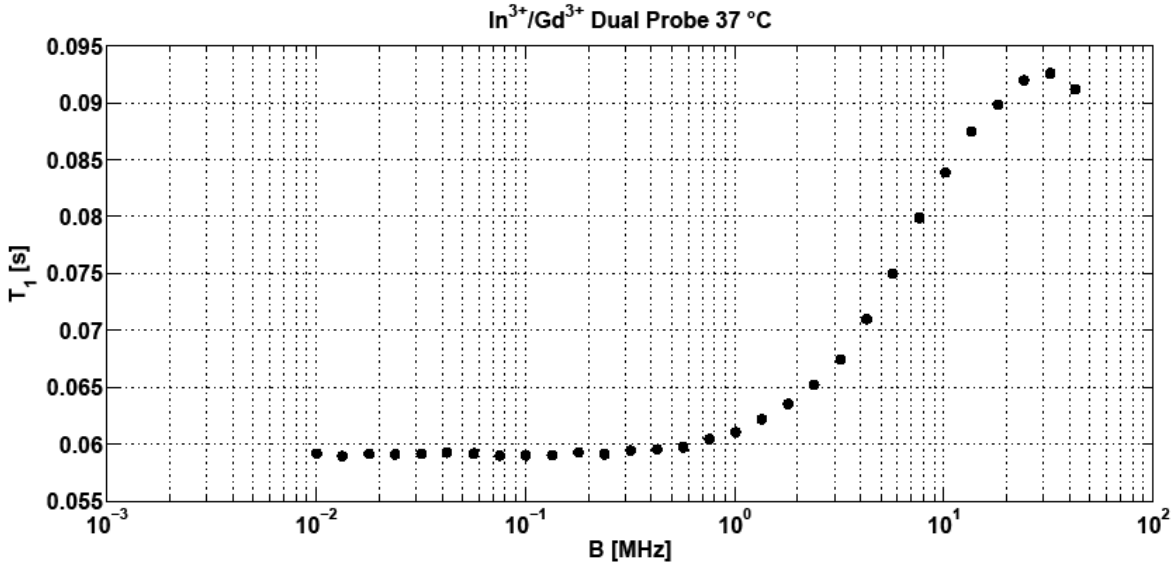

Figure S59: Dependence of T_1 relaxation time on the magnetic field strength for the Gd^{3+}/In^{3+} heterometallic complex **5c**, acquired at 37 °C.

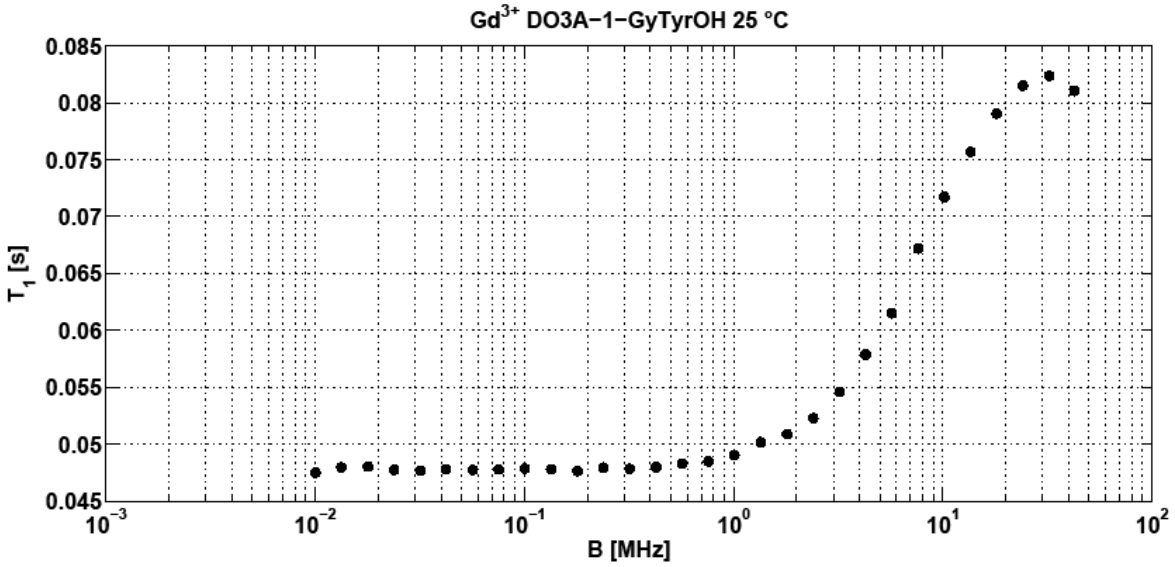

Figure S60: Dependence of T_1 relaxation time on the magnetic field strength for the alkyne building block **6b**, acquired at 25 °C.

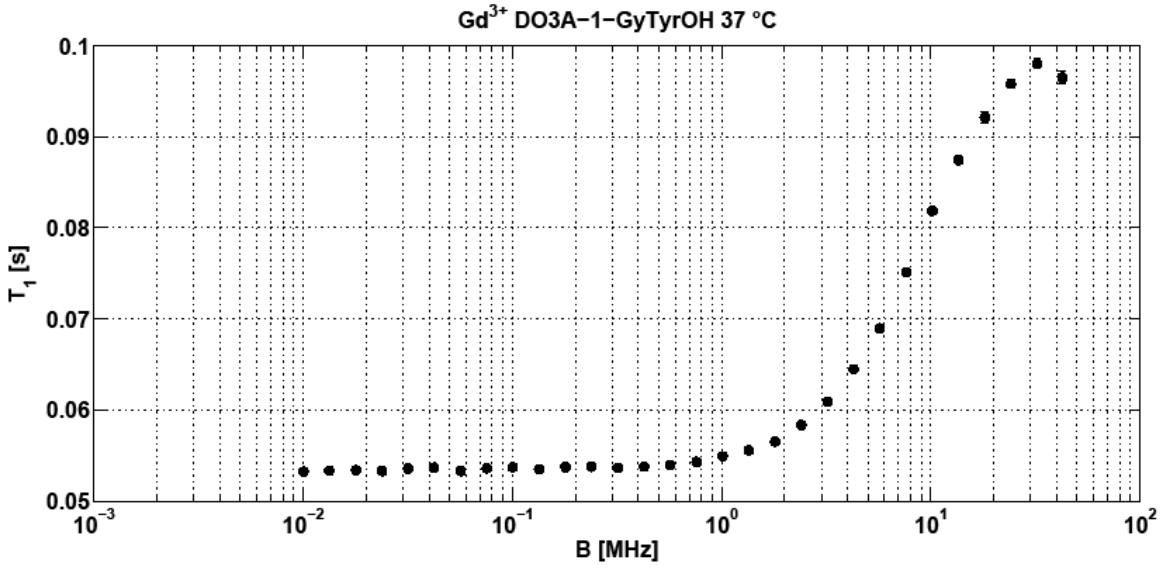

Figure S61: Dependence of T_1 relaxation time on the magnetic field strength for the alkyne building block **6b**, acquired at 37 °C.

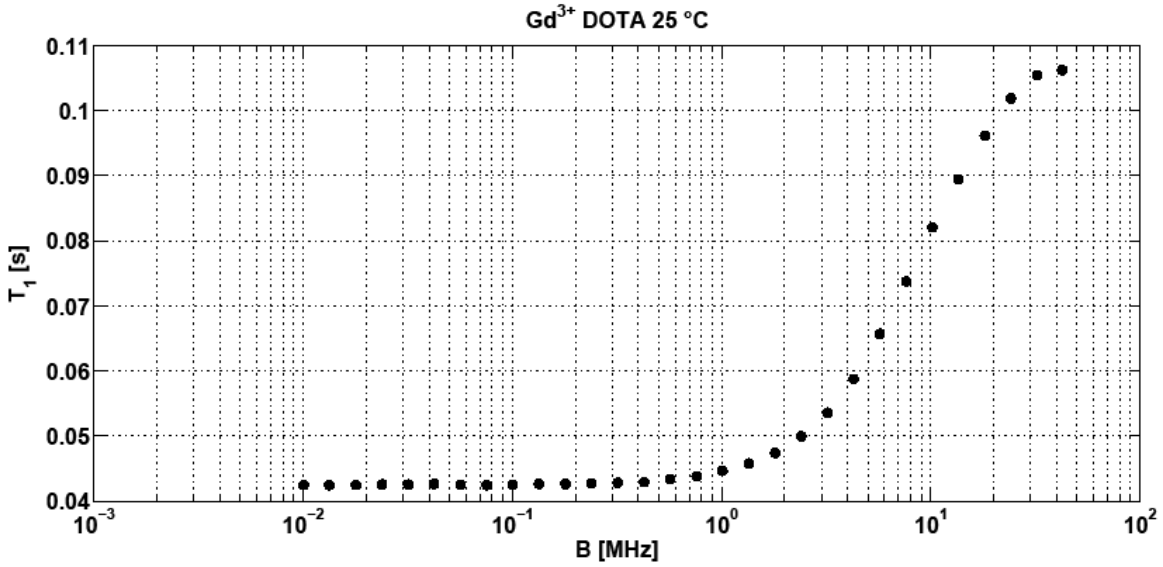

Figure S62: Dependence of T_1 relaxation time on the magnetic field strength for the commercial MRI contrast agent Dotarem (**16**), acquired at 25 °C.

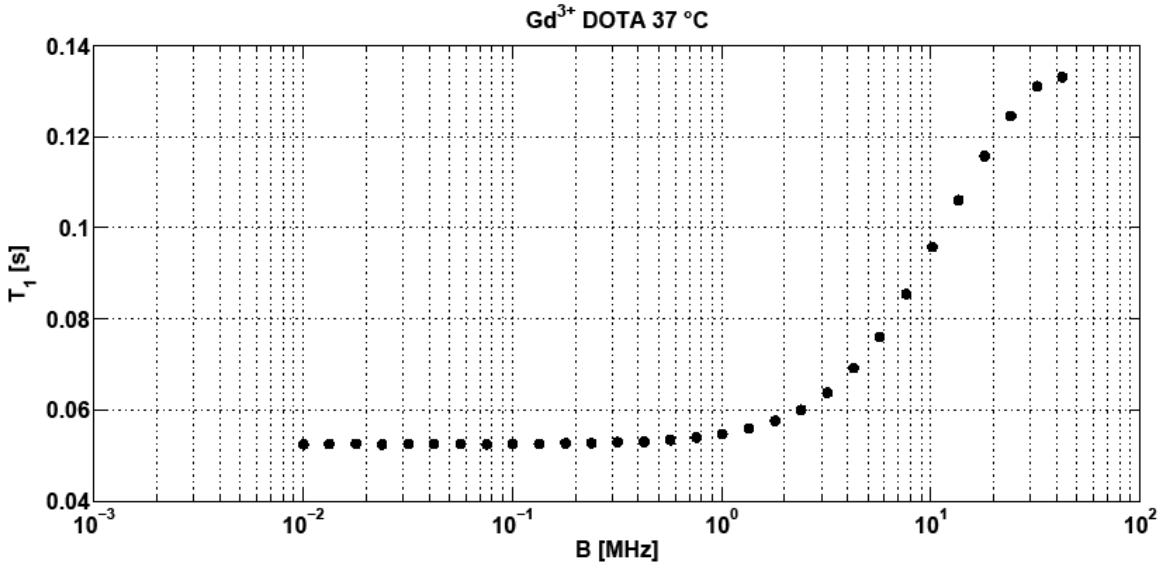

Figure S63: Dependence of T_1 relaxation time on the magnetic field strength for the commercial MRI contrast agent Dotarem (**16**), acquired at 37 °C.

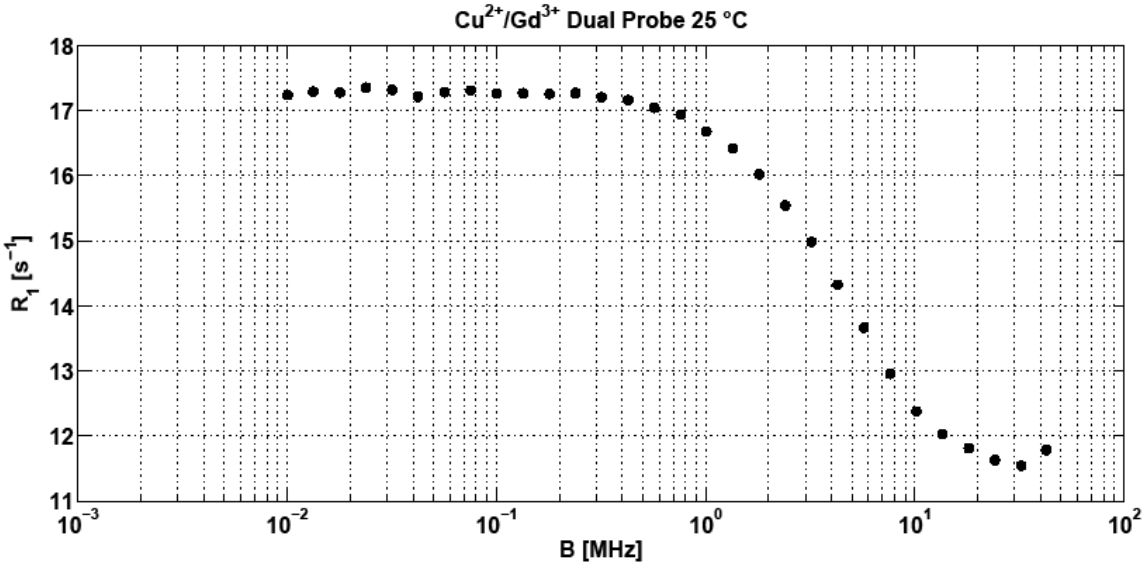

Figure S64: Dependence of R_1 relaxivity on the magnetic field strength for the Gd^{3+}/Cu^{2+} heterometallic complex **5a**, acquired at 25 °C.

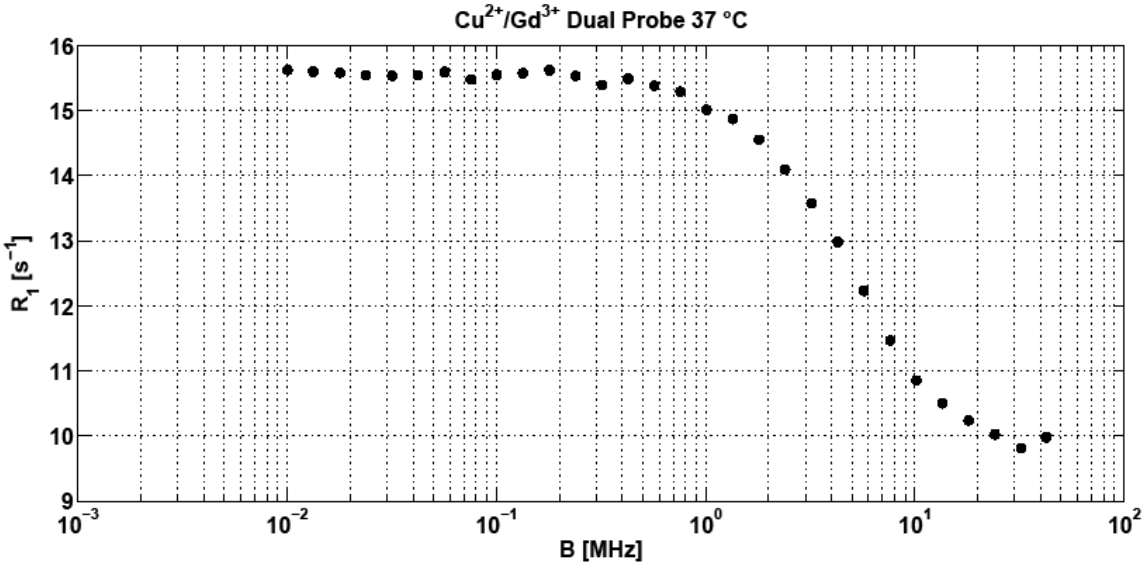

Figure S65: Dependence of R_1 relaxivity on the magnetic field strength for the Gd^{3+}/Cu^{2+} heterometallic complex **5a**, acquired at 37 °C.

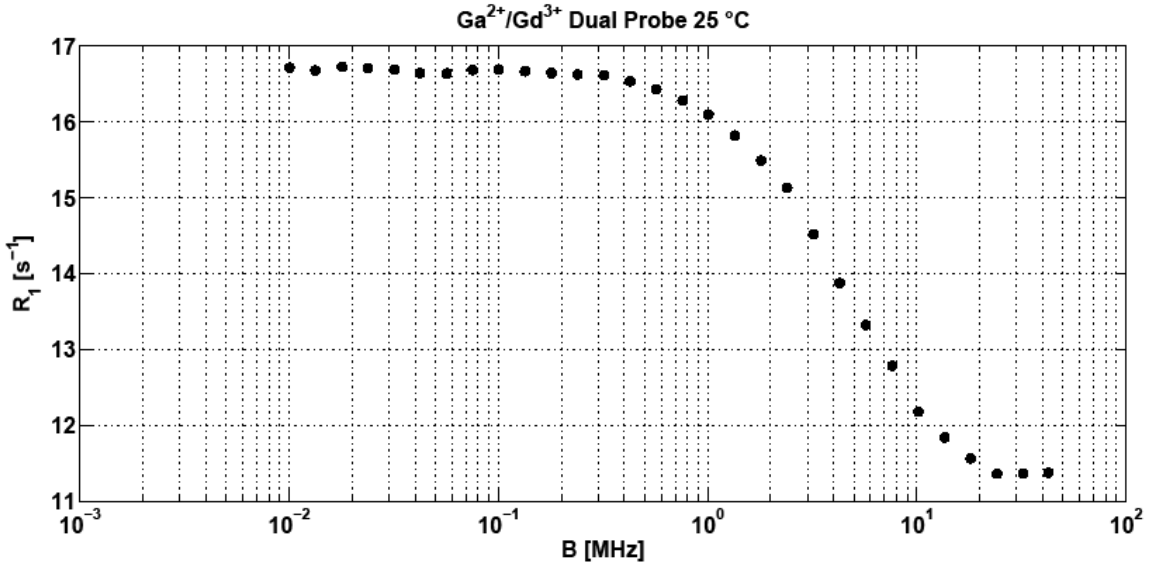

Figure S66: Dependence of R_1 relaxivity on the magnetic field strength for the Gd^{3+}/Ga^{3+} heterometallic complex **5b**, acquired at 25 °C.

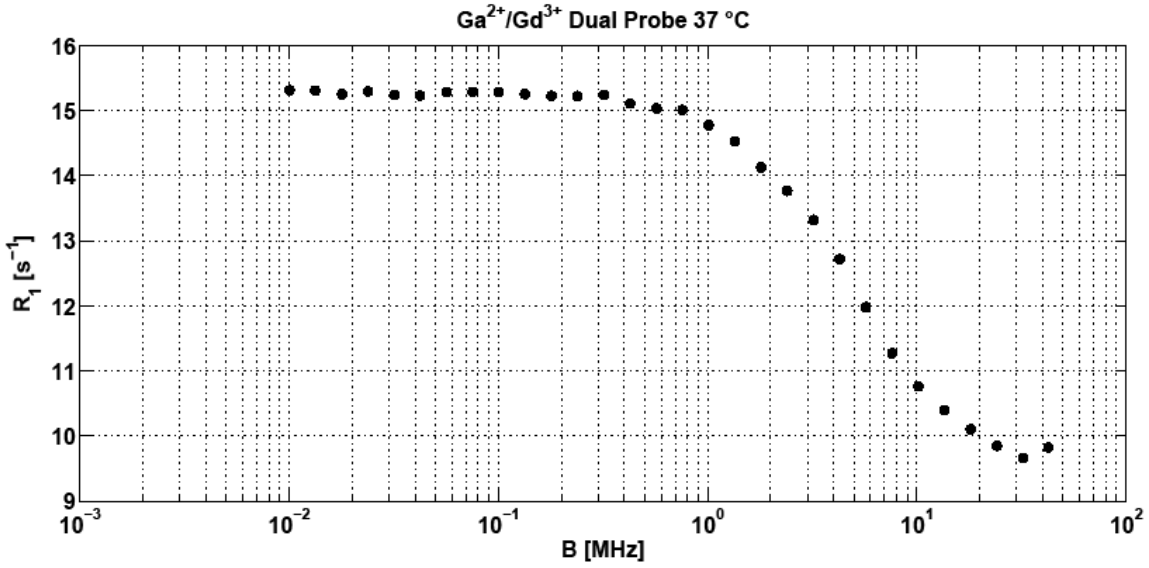

Figure S67: Dependence of R_1 relaxivity on the magnetic field strength for the Gd^{3+}/Ga^{3+} heterometallic complex **5b**, acquired at 37 °C.

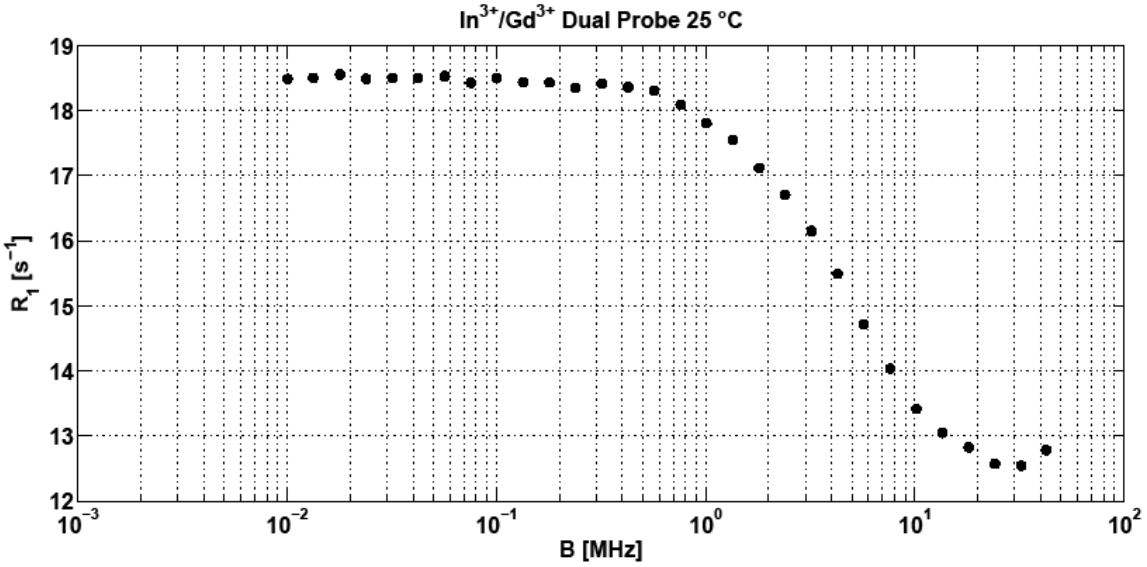

Figure S68: Dependence of R_1 relaxivity on the magnetic field strength for the Gd^{3+}/In^{3+} heterometallic complex **5c**, acquired at 25 °C. Related NMRD profile acquired at 37 °C is shown in the body of the paper (Figure 5).

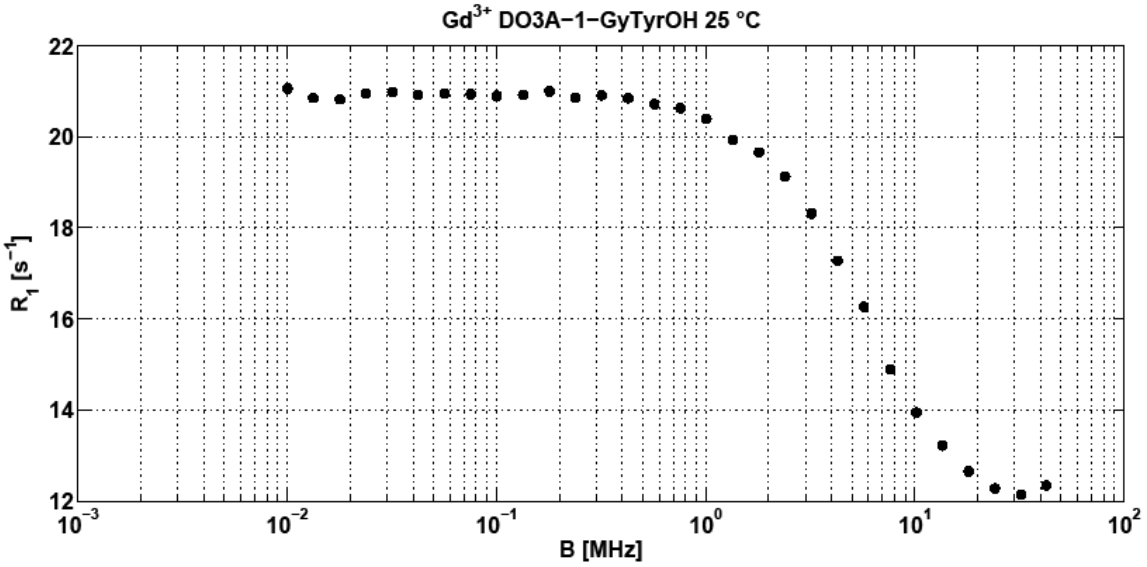

Figure S69: Dependence of R_1 relaxivity on the magnetic field strength for the alkyne building block **6b**, acquired at 25 °C.

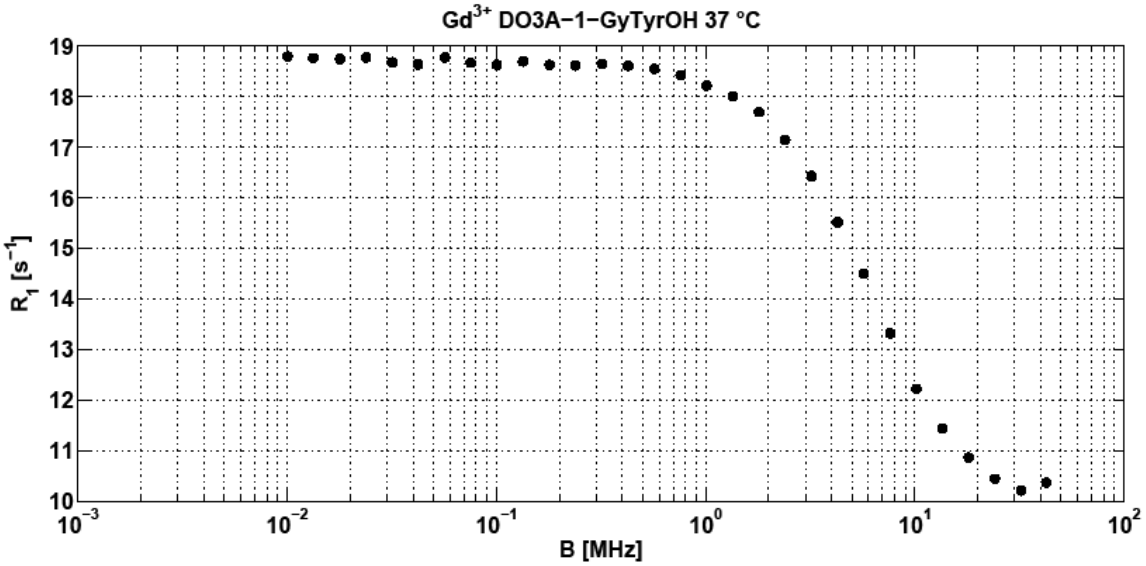

Figure S70: Dependence of R_1 relaxivity on the magnetic field strength for the alkyne building block **6b**, acquired at 37 °C.

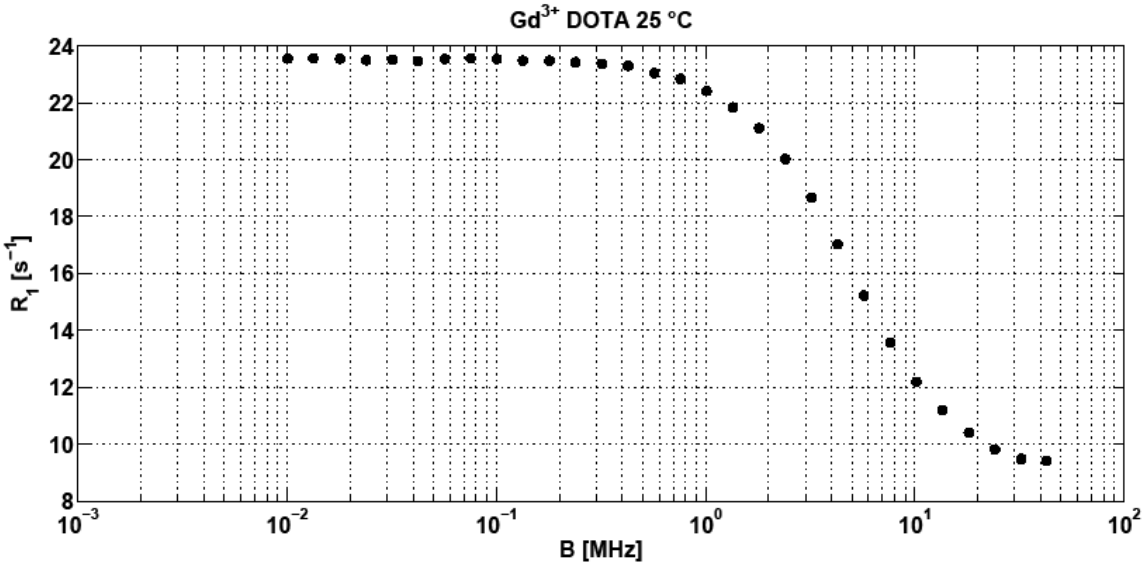

Figure S71: Dependence of R_1 relaxivity on the magnetic field strength for the commercial MRI contrast agent Dotarem (**16**), acquired at 25 °C. Related NMRD profile acquired at 37 °C is shown in the body of the paper (Figure 5)